

Quantum Error Source and Channel Coding

Dennis Lucarelli

*Department of Physics, American University, Washington DC**

A classical coding across a block of logical qubits is presented. We characterize subgroups of the product stabilizer group on a block of logical qubits corresponding to dual codes of classical error correcting codes. We prove conditions on the set of correctable error patterns allowing for unambiguous decoding based on a lookup table. For a large family of classical algebraic codes, we show that the qubit overhead required for syndrome extraction from L logical qubits scales as $\mathcal{O}(\log_2(L + 1))$, asymptotically. The basic construction is adapted to account for two-qubit and measurement errors, while still employing a lookup table based decoder. Moreover, we characterize the set of detectable errors and show how classical algebraic decoders can unambiguously locate logical qubits with errors even in the presence of syndrome noise. We argue that quantum error correction is more aptly viewed as source compression in the sense of Shannon, and that Shannon's source and channel coding theorems provide bounds on the overhead rates of quantum post-selection tasks, such as quantum error correction, at the level of the encoded quantum register.

I. INTRODUCTION

Quantum algorithms are known to achieve super-polynomial speedup in solving certain problems in discrete mathematics or as universal simulators of quantum systems [1]. Due to the fragility of quantum states, it is widely accepted that quantum error correction will be required to maintain quantum coherence for sufficiently long algorithm runtimes. However, circuit implementations of quantum algorithms of practical interest require billions, perhaps trillions, of time-steps. These so-called *deep* circuits necessitate a practically flawless error corrected or *logical* qubit—one that fails less than the reciprocal of the problem size. For a quantum algorithm with L logical qubits executing a depth Δ circuit, we require the probability of a logical qubit error $P_L < 1/\Delta L$. In principle, provided the underlying error rate is below a certain threshold [2], a logical qubit of arbitrarily high fidelity can be constructed by concatenating quantum codes [3]. However, code concatenation leads to an explosion of quantum resources (i.e. number of qubits) required to hold the data and the ancillary qubits needed for syndrome extraction and error correction. Recent studies suggest that an error corrected quantum computer will be very large, requiring millions of qubits [4–6], thereby placing the technology far beyond modern-day systems. Here, we show that qubit overhead can be significantly reduced by taking the *gestalt* view of quantum error correction (QEC). We construct a QEC protocol defined across the entire quantum computer and show that ancillary or *syndrome* qubits can carry error information from multiple logical qubits simultaneously. From the syndrome measurement results, collective inference can efficiently and provably reconstruct the errors unambiguously, even in the presence of measurement errors. Our construction is based on classical coding theory.

In the context of quantum communication over a Pauli

channel, the *hashing bound* [7] characterizes the achievable rate of transmitting k message qubits encoded in n physical qubits as asymptotically limited by the Shannon entropy of the channel $k/n < 1 - H_2(\mathbf{p})$. Here, $\mathbf{p} = [p_x, p_y, p_z]$ is a vector of Pauli channel error probabilities and $H_2(\mathbf{p})$ denotes Shannon's binary entropy function. This bound can be seen as a special case of the quantum channel capacity [8–10]. Moreover, using Shannon's methods of typicality and random code constructions, quantum stabilizer codes [11] can achieve the quantum channel capacity with a Pauli error model for large enough n [12]. Strictly speaking, however, QEC is not channel coding, as typically construed in the classical theory. In channel coding, a message's error syndrome is computed at the encoder, appended to the message and sent over a noisy channel. At the receiver, the decoder has access and utilizes *both* the noise corrupted message and syndrome to reconstruct the message. In QEC—as opposed to quantum communication—the decoder has access to the error syndrome only.

Up to an irrelevant phase, the Pauli group on n qubits $\mathcal{P}_n = \langle \pm iI, X, Y, Z \rangle^{\otimes n}$ is isomorphic to the binary vector space \mathbb{F}_2^{2n} with modulo 2 arithmetic and the symplectic inner product [13]. By this correspondence, syndrome extraction is equivalent to mapping a length $2n$ bit string (accounting for both X and Z -type errors) to a length $n - k$ bit syndrome, and thus performs compression of *classical* data—albeit *unknown* classical data derived from quantum data. This is the operational meaning of the hashing bound, which can be restated as Shannon's source coding theorem [14] for linear block codes bounding the optimal compression rate of binary data by the entropy of the random source, namely $n - k > nH_2(\mathbf{p})$. Here, \mathbf{p} parameterizes a Pauli *error source*. These remarks, though perhaps not framed as such in the quantum literature, are well known. Indeed, by source-channel coding duality, we may resolve the issue and recast QEC as channel coding since the decoder expects to receive the *zero message* (no errors) and hence the message is not needed. However, we find it advantageous to continue within the source coding framework.

* dgl@american.edu

Our contribution, from both an information theoretic and syndrome qubit overhead perspective, is that Shannon's bounds hold for blocks of logical qubits.

Given an error syndrome y and a linear error correcting code specified by the parity-check matrix H , the maximum-likelihood decoding problem is to determine the vector x with a minimum number of non-zero entries such that $Hx = y$. This inverse problem is known to be NP-hard for classical linear error correcting codes [15], implying that an efficient maximum-likelihood decoder is not likely to exist. Similar complexity arguments have been shown for quantum decoders [16, 17]. Further complicating the quantum decoding problem is that errors in the syndrome measurements are likely. This is an unavoidable consequence of faulty two-qubit gates and quantum measurements, which often have error rates orders of magnitude higher than data qubit errors. A number of methods have been proposed to account for syndrome measurement errors in quantum decoding, including minimum weight perfect matching decoders [18, 19] and iterative belief-propagation based decoders [20]. Here, we construct a lookup table decoder, designed for a restricted class of error patterns acting on a block of logical qubits, that can be queried with nearest-neighbor binary string matching to unambiguously determine the errors in the data qubits while also protecting against errors in the syndrome measurements.

Quantum product code constructions have been proposed previously in the literature. In [21], using the CSS construction, conditions were derived for obtaining a quantum error correcting code from the (direct) product of two classical error correcting codes. More recently, in [22], quantum tensor product codes, the quantum analogues of generalized tensor product codes [23, 24], where the constituent codes are defined over a field and an extension field were investigated. Notably, quantum hypergraph-product codes [25] employ the Kronecker product to construct a quantum parity check matrix from two classical codes. These product constructions encode multiple logical qubits in a single block of data qubits and define proper quantum error correcting codes. In contrast, as discussed in the following, the method proposed here, while based on a product code construction, is not strictly a quantum code. Rather, we propose the use of any binary, classical code linking multiple copies of a single quantum code.

Notation and background on quantum and classical error correcting codes may be found in Appendix A.

II. RESULTS

We propose a method that detects and locates errors in a length- L block of logical qubits by constructing stabilizer circuits acting on the entire block of logical qubits and collectively processing the syndrome measurement results. In particular, we construct stabilizers in the

product group

$$\mathcal{G} := \mathcal{S}_1 \times \mathcal{S}_2 \times \cdots \times \mathcal{S}_L \quad (1)$$

where \mathcal{S}_ℓ is the stabilizer group of a quantum error correcting code \mathcal{Q} acting on logical qubit ℓ . Let $\mathcal{Q} \sim [[n, k, d_Q]]$ denote a quantum code encoding k logical qubits in n physical qubits with code distance d_Q , and capable of correcting $t_Q = \lfloor \frac{d_Q-1}{2} \rfloor$ errors. Defining the total number of data qubits as $N = nL$, we have $\mathcal{G} \subset \mathcal{P}_N$.

Suppose we have a block of $L = 7$ logical qubits. For arbitrary $s \in \mathcal{S}$ and the identity e , consider the following elements of \mathcal{G}

$$\begin{aligned} & seseses \\ & esseess \\ & eeessss \end{aligned} \quad (2)$$

One may recognize the stabilizer elements $\{e, s\}$ arranged (columnwise) in the binary representation of the integers one through seven or, equivalently, according to the parity-check matrix of a classical Hamming $[7, 4, 3]$ error correcting code. The key observation is that this “encoding” is realized by the Kronecker product between a binary matrix and a parity-check matrix of a quantum error correcting code. In particular, the Pauli operator corresponding to the Kronecker product of any binary vector with the binary representation of a stabilizer generator is again in the product stabilizer \mathcal{G} . The ordering of the product is critical – post-multiplying by a binary matrix does not produce an element of the stabilizer. As commuting elements in \mathcal{G} , measurements of Pauli operators corresponding to rows of a matrix constructed by pre-multiplying a stabilizer by a binary matrix can be performed without leaving the codespace and destroying the quantum information held in the data qubits.

The canonical scheme for syndrome extraction from L logical qubits, where separate blocks of syndrome qubits are allocated to each logical qubit and each stabilizer, corresponds to a parity-check matrix $\mathbf{I}_L \otimes H_Q$ formed by the parity-check matrix for \mathcal{Q} and the $L \times L$ identity matrix. In contrast, our construction first selects a classical error correcting code \mathcal{C} with parameters $[L, M, d_C]$ and measures the stabilizers corresponding to rows of the matrix formed by the parity-check matrices of the classical code \mathcal{C} and the quantum code \mathcal{Q}

$$H_C \otimes H_Q \quad (3)$$

The layout of data qubits for performing error correction depends on the choice of quantum code and device architecture. Here, we conceptually arrange the data qubits in a rectangular array with each column corresponding to the data qubits comprising a logical qubit. Under the Pauli-to-binary isomorphism, unknown error patterns $[\mathbf{X} | \mathbf{Z}]^\top$ are then represented by $2n \times L$ binary matrices with constituent bit-flip \mathbf{X} and phase-flip \mathbf{Z} matrices of dimension $n \times L$. Our construction applies to CSS codes [26, 27], for which bit-flip and phase-flip

corrections can be performed independently, so, without loss of generality, we will denote an error pattern by the binary matrix \mathbf{E} , which may represent \mathbf{X} or \mathbf{Z} . The number of errors in the data qubits is given by the Hamming weight $wt(\mathbf{E})$, defined as the number of ones in the error pattern. When applied to a Pauli- X or Z operator, the Hamming weight is the number non-identity operators. The Hamming distance is the number of places that differ between two error patterns \mathbf{E} and \mathbf{E}' and is equivalent to $wt(\mathbf{E} \oplus \mathbf{E}')$. With a slight abuse of notation, the product $\mathbf{u} \otimes \mathbf{v}$ will denote both the Pauli operator obtained by performing the matrix Kronecker product applied to row vectors and its equivalent binary rectangular representation $\mathbf{v}^\top \mathbf{u}$.

A general error pattern may be expressed as a sum of weight-1 error patterns

$$\mathbf{E} = \bigoplus_{(q,\ell)} \mathbf{E}_{q\ell} \quad (4)$$

where $\mathbf{E}_{q\ell}$ has a single non-zero element at the (q, ℓ) -th entry and the pairs $(q, \ell) \in (\{1, 2, \dots, n\}, \{1, 2, \dots, L\})$. The action of syndrome extraction performed according to the parity-check matrix $H_C \otimes H_Q$ can be represented by the matrix products defined by the Kronecker product identity

$$H_C \otimes H_Q \text{vec}(\mathbf{E}) = \text{vec}(H_Q \mathbf{E} H_C^\top) \quad (5)$$

where $\text{vec}(\mathbf{E})$ denotes the vector representation of an error pattern obtained by stacking the columns of \mathbf{E} and arithmetic is modulo 2. Suppose $\mathbf{E} = \mathbf{E}_{q\ell}$ is a weight-1 error pattern, then

$$H_Q \mathbf{E}_{q\ell} = [\mathbf{0} \cdots \mathbf{0} \ \Sigma_q \ \mathbf{0} \cdots \mathbf{0}] \quad (6)$$

where the \mathcal{Q} -syndrome $\Sigma_q = H_Q \mathbf{e}_q^\top$ is the ℓ -th column of the matrix on the right-hand side and \mathbf{e}_q denotes a vector with a 1 in the q -th entry and zeros elsewhere. The classical parity-check matrix H_C acts on the rows of $H_Q \mathbf{E}_{q\ell}$. If the i -th entry of Σ_q is 1, the \mathcal{C} -syndrome $\Theta_\ell = H_C \mathbf{e}_\ell^\top$ appears as the i -th row of $H_Q \mathbf{E}_{q\ell} H_C^\top$ yielding

$$H_Q \mathbf{E}_{q\ell} H_C^\top = \Sigma_q \Theta_\ell^\top \quad (7)$$

The product syndrome Ξ of a general error pattern \mathbf{E} , with $wt(\mathbf{E}) > 1$, is a binary sum over weight-1 syndromes

$$\Xi = \bigoplus_{(q,\ell)} \Sigma_q \Theta_\ell^\top \quad (8)$$

A. Illustrative Example

As a concrete example, consider a block of logical qubits encoded in the three-qubit repetition code protecting against a single bit-flip acting on the codewords

$$|\bar{0}\rangle = |000\rangle \quad |\bar{1}\rangle = |111\rangle \quad (9)$$

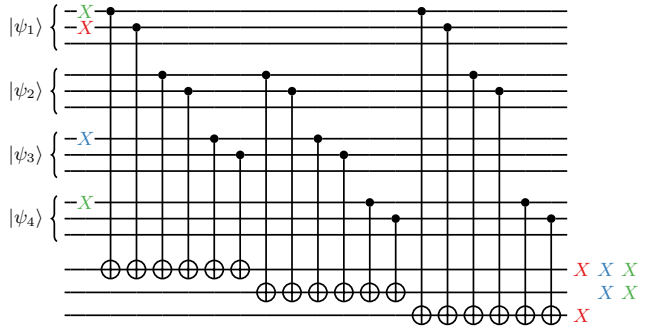


FIG. 1. Errors propagating through the circuit representation of $\mathbf{A}^\top \otimes [110]$ corresponding to the three-qubit bit-flip code stabilizer $s = ZZI$. Four logical qubits $|\psi_\ell\rangle$ enter the circuit and are subject to bit-flip errors (“X”) highlighted in color. Using the propagation rules of Pauli- X operators under CNOT gates, errors propagate to the syndrome qubits as shown in the lower right portion of the circuit.

The stabilizer group $\mathcal{S} = \langle ZZI, ZIZ \rangle$ is represented by the binary parity-check matrix

$$H_Q = \begin{bmatrix} 1 & 1 & 0 \\ 1 & 0 & 1 \end{bmatrix} \quad (10)$$

The Pauli- Z operator corresponding to the product $[1101] \otimes [110]$ is given by $ZZIZZIZIZZI$ which is an element of \mathcal{G} for the three-qubit bit-flip code. A construction that encodes 7 logical qubits is based on the classical $[7, 4, 3]$ Hamming code with parity-check matrix in systematic form given by

$$[I_3 \mid \mathbf{A}^\top] = \begin{bmatrix} 1 & 0 & 0 & 1 & 1 & 1 & 0 \\ 0 & 1 & 0 & 0 & 1 & 1 & 1 \\ 0 & 0 & 1 & 1 & 1 & 0 & 1 \end{bmatrix} \quad (11)$$

For brevity, we choose $H_C = \mathbf{A}^\top$ to encode 4 logical qubits and construct the parity-check matrices

$$\mathbf{A}^\top \otimes [110] = \begin{bmatrix} 1 & 1 & 0 & 1 & 1 & 0 & 1 & 1 & 0 & 0 & 0 & 0 \\ 0 & 0 & 0 & 1 & 1 & 0 & 1 & 1 & 0 & 1 & 1 & 0 \\ 1 & 1 & 0 & 1 & 1 & 0 & 0 & 0 & 0 & 1 & 1 & 0 \end{bmatrix}$$

$$\mathbf{A}^\top \otimes [101] = \begin{bmatrix} 1 & 0 & 1 & 1 & 0 & 1 & 1 & 0 & 1 & 0 & 0 & 0 \\ 0 & 0 & 0 & 1 & 0 & 1 & 1 & 0 & 1 & 1 & 0 & 1 \\ 1 & 0 & 1 & 1 & 0 & 1 & 0 & 0 & 0 & 1 & 0 & 1 \end{bmatrix}$$

Stabilizer circuits are constructed by coupling the data qubits to the syndrome qubits as specified by a parity-check matrix in the usual way: a two-qubit gate is added to the circuit from data qubit j to syndrome qubit i if and only if the (i, j) -entry of the parity-check matrix is 1. Returning to the example, FIG. 1 and 2 show stabilizer circuits of ZZI and ZIZ encoded with \mathbf{A}^\top . Four logical qubits $|\psi_\ell\rangle$, encoded in the three-qubit bit-flip code, enter the circuit and are subject to errors. There are a total

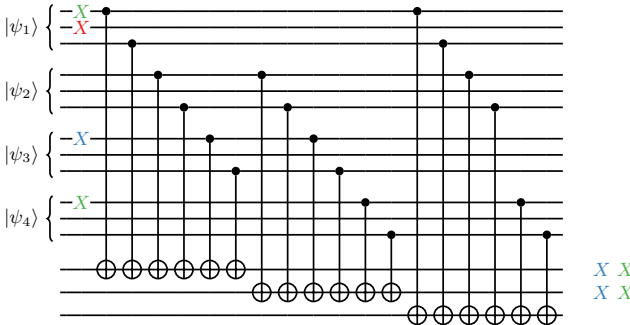


FIG. 2. Errors propagating through the circuit representation of $\mathbf{A}^\top \otimes [101]$ corresponding to the three-qubit bit-flip code stabilizer $s = ZIZ$. Four logical qubits $|\psi_\ell\rangle$ enter the circuit and are subject to bit-flip errors “X” highlighted in color. Errors propagate to the syndrome qubits as shown in the lower right portion of the circuit. Note that ZIZ does not couple the second data qubit to the syndrome qubits and, thus, the X_2 (red) does not propagate to the syndrome qubits.

of 12 data qubits (indexed from top to bottom) and 3 syndrome qubits per stabilizer. Using the propagation rules of Pauli- X operators under CNOT gates, we may track the errors through the circuit and observe how the parity relations defined by \mathbf{A}^\top manifest in the syndrome qubits. Let E_j denote an E -type Pauli error on data qubit j . A bit-flip occurring on the second physical qubit X_2 (red “X”) is coupled to the first and third syndrome qubit and a measurement in the Z basis will yield the binary outcomes $[101]$ (red “X” on syndrome qubits one and three). Similarly, an error on X_7 (blue “X”) propagates to the first and second syndrome qubit as dictated by the seventh column of $\mathbf{A}^\top \otimes [110]$. As in the classical case, there is ambiguity whenever the number of errors exceeds the correction radius $t_Q = 1$ as evident by the weight-2 error X_1X_{10} (green) producing syndrome measurement outcomes identical to the single qubit error X_7 (blue). The circuit couples the weight-2 error to the third syndrome qubit twice, negating the propagation of the error to that syndrome qubit.

Syndrome ambiguity may be understood by examining the cosets of the Pauli- X subgroup $\mathcal{P}_{12} = \{I, X\}^{\otimes 12}$ under the action of the Pauli- Z operator corresponding to $\mathbf{A}^\top \otimes [110]$. In the rectangular representation, the syndrome conflict depicted in FIG. 1 is produced by the error patterns

$$X_7 \simeq \begin{bmatrix} 0 & 0 & 1 & 0 \\ 0 & 0 & 0 & 0 \\ 0 & 0 & 0 & 0 \end{bmatrix} \quad X_1X_{10} \simeq \begin{bmatrix} 1 & 0 & 0 & 1 \\ 0 & 0 & 0 & 0 \\ 0 & 0 & 0 & 0 \end{bmatrix} \quad (12)$$

Both error patterns are within the correction radius $t_Q = 1$ for \mathcal{Q} (weight-1 errors on $|\psi_3\rangle$ and $\{|\psi_1\rangle, |\psi_4\rangle\}$ respectively) but the weight-2 error X_1X_{10} is greater the correction radius $t_C = 1$ for the classical code \mathcal{C} . This results in identical first rows of Θ^\top for both error patterns

under the action of H_C^\top

$$[0 \ 0 \ 1 \ 0] \mathbf{A} = [1 \ 0 \ 0 \ 1] \mathbf{A} = [1 \ 1 \ 0] \quad (13)$$

In other words, the row vectors $[0010]$ and $[1001]$ are in the same coset of \mathbf{A} . The measured syndromes “after” the action of the stabilizer $[110]$ will be identical and lead to a conflict.

A lookup table decoder exists for a class of errors \mathbb{E} if there’s a one-to-one mapping from syndrome measurements to error patterns from that class. Some quantum codes are degenerate, in the sense that multiple error patterns may result in the same syndrome measurement but can all be corrected by a single Pauli correction operator. For degenerate codes, the lookup table is modified to contain error syndrome-correction operator pairs. In either case, a lookup table may be pre-computed by iterating through all correctable error patterns $\mathbf{E} \in \mathbb{E}$ and using the binary matrix relation $H_Q \mathbf{E} H_C^\top$ to simulate the syndrome measurement outcomes. To construct the lookup table decoder, we must choose a single error operator from each coset, the *coset leader*, to represent the coset corresponding to a measured syndrome. A table of syndrome-coset pairs with the cosets ordered with the coset representative in the first column is known as a *standard array*. Portions of the standard arrays corresponding to syndrome extraction performed according to $\mathbf{A}^\top \otimes [110]$ and $\mathbf{A}^\top \otimes [101]$ are shown in Tables B.VIII and B.IX in the Appendix B. A lookup table decoder for single bit-flips may be constructed by joining these tables as shown in Table B.X. When syndrome extraction for all stabilizers is performed in parallel via $H_C \otimes H_Q$ each row of product syndrome Ξ corresponds to a different stabilizer and the flattened product syndrome as shown in Table B.X can be obtained by performing $\text{vec}(\Xi^\top)$. Assuming perfect CNOT gates and measurements, the lookup table decoder simply queries the keys of the table with the full syndrome measurement and returns the unique data qubit corresponding to the matched key to be corrected.

B. Subgroups of \mathcal{G}

Generators of the product stabilizer group \mathcal{G} may be expressed in terms of Kronecker products

$$\mathcal{G} = \langle \mathbf{e}_\ell \otimes s \rangle \quad (14)$$

Using the aforementioned isomorphism, we will interpret mixed products between binary vectors ($\mathbf{e}_\ell \in \mathbb{F}_2^L$) and Pauli operators ($s \in \mathcal{P}_n$) as well defined by implicitly mapping Pauli operators to their binary representation, performing the matrix Kronecker product applied to row vectors, and mapping the result back to Pauli operators.

A Pauli operator that commutes with the stabilizer group leaves the code space invariant and is unobservable during syndrome extraction. These operators form a normal subgroup of the Pauli group generated by $n+k$

operators known as the *normalizer* $\mathcal{N}(\mathcal{S})$ of \mathcal{S} in \mathcal{P}_n . Stabilizers and logical qubit rotations are in the normalizer as are non-trivial error patterns that go undetected during syndrome extraction. A code's distance, defined as the minimal weight Pauli operator in $\mathcal{N}(\mathcal{S}) \setminus \mathcal{S}$, is the distinguishing parameter of a quantum codes, as it determines the maximum weight of detectable and correctable errors. As such, one must characterize the structure of the normalizer to determine the error correcting capabilities of a quantum code. The normalizer $\mathcal{N}(\mathcal{G})$ of the product group \mathcal{G} is generated by

$$\mathcal{N}(\mathcal{G}) = \langle \mathbf{e}_\ell \otimes \eta_a \rangle \quad (15)$$

where $\eta_a \in \mathcal{N}(\mathcal{S})$ and $a \in \{1, 2, \dots, n+k\}$.

In classical coding theory, the rows $\{h_r\}$ of the parity-check matrix H_C form a vector space \mathcal{C}^\perp of dimension $R := L - M$ known as the *dual code* of \mathcal{C} . For all $s \in \mathcal{S}$ and $r \in \{1, 2, \dots, R\}$, the operators

$$\mathcal{H} := \langle h_r \otimes s \rangle \quad (16)$$

generate a proper subgroup of \mathcal{G} . To see this, note that $h \otimes s = \prod_{\ell'} \mathbf{e}_{\ell'} \otimes s \in \mathcal{G}$ where the ℓ' -th component of h is non-zero and \mathcal{H} is strictly contained in \mathcal{G} since the weight-1 vector $\mathbf{e}_\ell \notin \mathcal{C}^\perp$ for any code of distance greater than 1. Group multiplication (\odot) of generators of \mathcal{H} (and \mathcal{G}) in Kronecker form is defined by applying the distributive property of the Kronecker product over multiplication in \mathcal{P}_n and binary addition in \mathbb{F}_2^L to obtain

$$h \otimes s \odot h' \otimes s' = h \oplus h' \otimes ss' \cdot h \otimes s' \cdot h' \otimes s \quad (17)$$

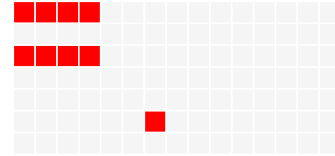
and is closed in \mathcal{H} since $h \oplus h' \in \mathcal{C}^\perp$ and $ss' \in \mathcal{S}$ (and $h \otimes s', h' \otimes s \in \mathcal{H}$). When $h = h'$, the product is defined as $h \otimes s \odot h \otimes s' = h \otimes ss'$, and when $s = s'$, $h \otimes s \odot h' \otimes s = h \oplus h' \otimes s$. Up to a rearrangement of rows, \mathcal{H} is the product subgroup corresponding to $H_C \otimes H_Q$.

As elements of \mathcal{P}_N , operators commute if and only if their binary representations are orthogonal under the symplectic inner product. For CSS codes, the symplectic inner product simplifies to the modulo 2 inner product between the binary representations of an *X*-type and a *Z*-type Pauli operator. Thus, the normalizer of the product subgroup \mathcal{H} is the set of Pauli operators in the kernel of $H_C \otimes H_Q$, or equivalently, binary matrices \mathbf{N} such that $H_Q \mathbf{N} H_C^\top = \mathbf{0}$. Let $\{g_m\}$ denote a basis of the classical code \mathcal{C} satisfying $g_m H_C^\top = \mathbf{0}$ for $m \in \{1, 2, \dots, M\}$. The normalizer $\mathcal{N}(\mathcal{H})$ is generated by a set of *column generators* $\mathbf{e}_\ell \otimes \eta_a$, so called because η_a appears in the ℓ -th column in the rectangular representation, and for $E_q \in \{X_q, Z_q\}$, a set of *row generators* $g_m \otimes E_q$ where g_m is the q -th row in the rectangular representation. Any product of row or column generators is an element of the normalizer as are cross products of the form $g \otimes \eta$. Also in the normalizer are non-identity Pauli operators satisfying the conditions

$$H_Q \mathbf{N} \subset \mathcal{C} \quad \mathbf{N} H_C^\top \subset \mathcal{N}(\mathcal{S}) \quad (18)$$

where the matrices are viewed as collections of rows (left) or columns (right).

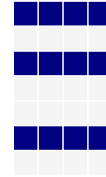
As a non-trivial example of this type of normalizer, consider a block of 15 Steane [27] logical qubits encoded with the $[15, 11, 3]$ classical Hamming code. A weight-9 normalizer element \mathbf{N} (say of *X*-type) may be illustrated as



where the red squares mark error locations. Under the action of H_Q , \mathbf{N} transforms to



from which it is evident that the non-zero columns of \mathbf{N} lie in the same coset of H_Q and map to identical columns of $H_Q \mathbf{N}$, producing rows in \mathcal{C} . Similarly, \mathbf{N} transforms to



with columns in $\mathcal{N}(\mathcal{S})$ under the action of H_C^\top .

Operators satisfying (18) can be written in terms of row and column generators. The left-hand condition implies

$$H_Q \mathbf{N} = \bigoplus_{(m,i)} g_m \otimes E_i = \bigoplus_{(m,i)} g_m \otimes H_Q \mathbf{v}_i \quad (19)$$

where $i \in \{1, 2, \dots, n-k\}$ and \mathbf{v}_i is such that $H_Q \mathbf{v}_i = E_i$. The right-hand condition implies

$$\mathbf{N} H_C^\top = \bigoplus_{(r,a)} \mathbf{e}_r \otimes \eta_a = \bigoplus_{(r,a)} H_C \mathbf{u}_r \otimes \eta_a \quad (20)$$

where $r \in \{1, 2, \dots, R\}$ and \mathbf{u}_r is such that $H_C \mathbf{u}_r = \mathbf{e}_r$, collectively yielding

$$\mathbf{N} = \bigoplus_{(m,i)} g_m \otimes \mathbf{v}_i \quad \bigoplus_{(r,a)} \mathbf{u}_r \otimes \eta_a \quad (21)$$

Summarizing, we have identified a dependent set of $L(n+k) + 2Mn$ operators

$$\mathcal{N}(\mathcal{H}) = \langle \mathbf{e}_\ell \otimes \eta_a, g_m \otimes E_q \rangle \quad (22)$$

and established the subgroups $\mathcal{H} \subset \mathcal{G}$, $\mathcal{N}(\mathcal{G}) \subset \mathcal{N}(\mathcal{H})$,

$$\mathcal{L} := \mathcal{P}_N / \mathcal{N}(\mathcal{H}) \subset \mathcal{P}_N / \mathcal{N}(\mathcal{G}) \quad (23)$$

C. Main Result

The form of the generators of $\mathcal{N}(\mathcal{H})$ elucidates the structure of the quotient group \mathcal{L} . The minimum weight of the non-stabilizer elements of $\mathcal{N}(\mathcal{H})$ is the distance of \mathcal{Q} since we assume $d_C \geq d_Q$ and $wt(\mathbf{e}_\ell \otimes \eta_a) = wt(\mathbf{e}_\ell) \cdot wt(\eta_a) \geq d_Q$. Thus, we immediately recover the detectability condition of the quantum code \mathcal{Q} , namely, the number of errors in a logical qubit must be strictly less than d_Q to anti-commute and be detectable. For this reason, our construction is not a quantum code, *per se*, but more aptly described as a hybrid classical-quantum coding scheme.

Let $\mathbf{E}_{*\ell}$ denote the ℓ -th column of \mathbf{E} (the error pattern on the ℓ -th logical qubit) and $wt_c(\mathbf{E})$ the number of non-zero columns of \mathbf{E} . A Pauli operator that negates either normalizer condition (18) anti-commutes with \mathcal{H} and is detectable. If $wt_c(\mathbf{E}) < d_C$, then the weights of the rows of $H_Q \mathbf{E}$ must be less than d_C and cannot be in a code \mathcal{C} with minimum weight d_C . Similarly, $wt(\mathbf{E}_{*\ell}) < d_Q$ for any ℓ implies $\mathbf{E} H_C^\dagger \notin \mathcal{N}(\mathcal{S})$. The main result is simply stated:

A lookup table decoder exists for an encoding with $H_C \otimes H_Q$ if the number of logical qubits with errors (of each error type) is not greater than t_C and the number of errors in each logical qubit is not greater than t_Q .

Our claim is that all error patterns from the set

$$\mathbb{E} = \left\{ \mathbf{E} \in \{ \mathbf{X}, \mathbf{Z} \} \mid wt(\mathbf{E}_{*\ell}) \leq t_Q \forall \ell, wt_c(\mathbf{E}) \leq t_C \right\} \quad (24)$$

are correctable. The first condition $wt(\mathbf{E}_{*\ell}) \leq t_Q$ is familiar from QEC theory. Coding via $H_C \otimes H_Q$ adds the second condition enforcing a constraint across the block of logical qubits. To prove the result, it suffices to show that each error pattern in \mathbb{E} is the coset leader of the coset to which it belongs or, equivalently, that for $\mathbf{E} \in \mathbb{E}, \mathbf{N} \in \mathcal{N}(\mathcal{H})$, then $\mathbf{E} \oplus \mathbf{N} \notin \mathbb{E}$. Note that the Hamming distance can be written as $wt(\mathbf{E} \oplus \mathbf{N}) = wt(\mathbf{E}) + wt(\mathbf{N}) - 2wt(\mathbf{EN})$ where \mathbf{EN} denotes component-wise multiplication, showing that adding a non-zero \mathbf{N} to \mathbf{E} adds weight except where non-zero entries align. Suppose $\mathbf{E} = \mathbf{a} \otimes \mathbf{b}$ with $wt(\mathbf{a}) \leq t_C$ and $wt(\mathbf{b}) \leq t_Q$, then $\mathbf{E} \in \mathbb{E}$, and, without loss of generality, let $\mathbf{N} = g \otimes \mathbf{b}$ for some $g \in \mathcal{C}$. Then, by the multiplication rules for \mathcal{G} (see 17), $wt(\mathbf{E} \oplus \mathbf{N}) = wt(\mathbf{a} \oplus g)wt(\mathbf{b})$, and since $wt(\mathbf{a} \oplus g) \geq d_C - wt(\mathbf{a}) \geq d_C - t_C \geq t_C + 1$, we have $wt_c(\mathbf{E} \oplus \mathbf{N}) > t_C$ and $\mathbf{E} \oplus \mathbf{N} \notin \mathbb{E}$. Similarly, if $\mathbf{N}' = \mathbf{a} \otimes \eta$ for some $\eta \in \mathcal{N}(\mathcal{S})$, then $wt(\mathbf{E} \oplus \mathbf{N}') = wt(\mathbf{a})wt(\mathbf{b}\eta)$, and since $wt(\mathbf{b}\eta) \geq d_Q - wt(\mathbf{b}) \geq d_Q - t_Q \geq t_Q + 1$. For any non-zero index ℓ' of \mathbf{a} , we have $wt((\mathbf{E} \oplus \mathbf{N}')_{*\ell'}) > t_Q$ and $\mathbf{E} \oplus \mathbf{N}' \notin \mathbb{E}$. For arbitrary $\mathbf{E} \in \mathbb{E}$ and $\mathbf{N} \in \mathcal{N}(\mathcal{H})$, the result follows from linearity.

D. Product Source Coding

The basic construction is now cast in the framework of Shannon's source coding theorem. We view each data qubit as a memoryless random information source emitting symbols from the discrete alphabet of Pauli operators $\{I, X, Y, Z\}$. While not strictly necessary, we model Pauli errors with independent Bernoulli random variables $\{\mathcal{X}, \mathcal{Y}, \mathcal{Z}\}$ with probabilities $p_x = P(\mathcal{X} = X)$, $p_y = P(\mathcal{Y} = Y)$, $p_z = P(\mathcal{Z} = Z)$, respectively. When $p_x = p_y = p_z$, our error model is equivalent to the familiar depolarizing channel by source and channel coding duality, as noted in the Introduction. All quantum error correcting codes are compressive when viewed as a mapping from error patterns to binary syndrome measurements: for each error type, the Steane $[[7, 1, 3]]$ code compresses a 7 dimensional error vector into 3 syndrome bits, and $[[17, 1, 5]]$ topological color codes compress a 17 dimensional error vector into 8 syndrome bits. Here, we stress the compressive properties of quantum and classical error correcting codes and refer to an encoding with $H_C \otimes H_Q$ as *Quantum Error Source Coding*.

In his seminal work [14], Shannon defined a precise measure of the information content of a random source \mathcal{X} in terms of a logarithmic function $H_2(\mathcal{X})$, commonly referred to as the *Shannon entropy*. Informally, Shannon's source coding theorem states that N independent, identically distributed (i.i.d) random variables \mathcal{X} can be compressed into $NH_2(\mathcal{X})$ bits with negligible probability of information loss. It is often remarked that quantum error correction is analogous to a heat engine transferring entropy from data qubits, hot with noise, to cold syndrome qubits. By the use of a classical error correcting code across a block of logical qubits, our construction makes this notion concrete and shows that the overhead needed for syndrome extraction for the entire computer is ultimately limited by the Shannon entropy of the error source, which is typically much less than 1.

Any binary, linear code can be used in the construction. For example, we may choose \mathcal{C} from the Bose-Chaudhuri-Hocquenghem (BCH) family of codes [28] and \mathcal{Q} as the Steane code ($t_Q = 1$). While not achieving Shannon's source compression limit, the BCH family has the asymptotic code parameters $[L, L - t_C \lceil \log_2(L + 1) \rceil, 2t_C + 1]$. Using a t_C -error correcting BCH code with large enough L , our construction requires only $\mathcal{O}(\log_2(L + 1))$ extra qubits for syndrome extraction. In the canonical approach to QEC, each logical qubit operates independently and L Steane logical qubits functioning as a block code corresponds to an L -error correcting code in our framework. Here, we limit the number of logical qubits with errors to $t_C \ll L$, but achieve an exponential reduction in the number of syndrome qubits needed to perform quantum error correction, asymptotically.

Syndrome qubit overhead from constructions formed by $[L, M, d_C]$ BCH codes and the $[[7, 1, 3]]$ Steane and $[[17, 1, 5]]$ color code are shown in FIG. 3. The BCH codes

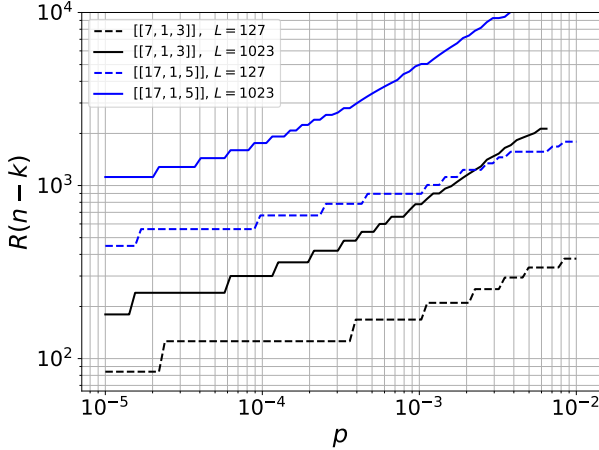


FIG. 3. Overhead plots for product source coding with $[L, M, d_c]$ BCH codes and the $[[7, 1, 3]]$ Steane and $[[17, 1, 5]]$ color codes. The number of syndrome qubits $R(n-k)$, where $R = L - M$ and $(n - k) = |\mathcal{S}|$, is plotted versus the Pauli error rate p .

were chosen from families with $L = 127$ and $L = 1023$ with sufficient distance such that the failure probability is close to its minimum (see Sec. II D 1). The product code overhead $R(n-k)$ compares favorably against the canonical approach where $L(n-k)$ syndrome qubits are required. For example, measuring 16 stabilizers of the color code from $L = 127$ logical qubits would require 2032 syndrome qubits in the canonical scheme, but in the low noise regime, say $p = 10^{-4}$, the BCH-color product code requires just 672. In general, compression by H_C is characterized by the rate of the classical code M/L . The block length scaling of BCH codes is evident as L increases: at the error rate $p = 10^{-4}$, a computation with 1023 color code logical qubits requires an overhead of 1760 qubits, less than a threefold increase over a system with 127 logical qubits.

1. Failure Probability

The lookup table decoder will fail to correct any error pattern not in \mathbb{E} , and thus the protocol fails with probability

$$P_F = LP(wt(\mathbf{E}_{*\ell}) > t_Q) + P(wt_c(\mathbf{E}) > t_C) - LP(wt(\mathbf{E}_{*\ell}) > t_Q)P(wt_c(\mathbf{E}) > t_C) \quad (25)$$

Assuming independent errors, the first term of P_F is the probability that any logical qubit suffers errors exceeding t_Q . For Bernoulli sources with probability p , we have

$$P(wt(\mathbf{E}_{*\ell}) > t_Q) = 1 - \sum_{\tau=1}^{t_Q} \binom{n}{\tau} p^\tau (1-p)^{n-\tau} \quad (26)$$

\mathcal{Q}	$p = 10^{-3}$	$p = 10^{-4}$	$p = 10^{-5}$
$[[7, 1, 3]]$	2e-05 (3e-08)	2e-07 (3e-11)	2e-09 (3e-14)
$[[17, 1, 5]]$	7e-07 (6e-12)	7e-10 (1e-16)	7e-13 (1e-16)
$[[23, 1, 7]]$	9e-09 (2e-16)	9e-13 (1e-16)	1e-16 (1e-16)

TABLE I. Comparison of probabilities of a high weight error pattern exceeding the correction radius $P(wt(\mathbf{E}_{*\ell}) > t_Q)$ and the distance $P(wt(\mathbf{E}_{*\ell}) \geq d_Q)$ (in parentheses) for a Steane, color and Golay logical qubit with Pauli error rates $p = 10^{-3}, 10^{-4}$, and 10^{-5}

In the canonical scheme, $LP(wt(\mathbf{E}_{*\ell}) > t_Q)$ is an estimate of the failure rate, assuming perfect two-qubit gates and measurements. Table I compares $P(wt(\mathbf{E}_{*\ell}) > t_Q)$ for a Steane, color, and $[[23, 1, 7]]$ Golay logical qubit.¹

For a logical qubit with n data qubits and a Pauli error probability p , the probability of at least one error in a logical qubit is given by $p_\ell = 1 - (1 - p)^n$, and the second term in P_F (25) is binomial with probability p_ℓ

$$P(wt_c(\mathbf{E}) > t_C) = 1 - \sum_{\tau=1}^{t_C} \binom{L}{\tau} p_\ell^\tau (1 - p_\ell)^{L-\tau} \quad (27)$$

Since error patterns exceeding the quantum correction radius t_Q will cause a failure, the probabilities (scaled by L) in Table I serve as lower bounds on P_F . Therefore, given a estimate of p , a good choice for the classical code \mathcal{C} is one with sufficient distance such that

$$P(wt_c(\mathbf{E}) > t_C) \sim \mathcal{O}(LP(wt(\mathbf{E}_{*\ell}) > t_Q)) \quad (28)$$

This methodology was followed to compute the overhead rates shown in FIG. 3.

Failure probabilities (25) computed with $L = 127$ and the binomial probabilities (26) and (27) are plotted against physical error rates in FIG. 4. For each quantum code shown, a single length-127 t_C -BCH code satisfying the criterion (28) was chosen assuming $p = 10^{-4}$. For example, we observe that 127 color code qubits can achieve a logical failure rate of $\mathcal{O}(10^{-7})$ at the cost of 672 syndrome qubits (FIG. 3) required to correct both X and Z -type errors occurring with probability 10^{-4} . As noted in the Introduction, the inverse of the failure rate is a rough estimate of feasible circuit depth. Our failure probability accounts for *any* logical error, so here we have $\Delta \sim 1/P_F$, and observe that product code constructions with $\mathcal{O}(10^2)$ color or Golay logical qubits approach feasibility for running error-free deep circuits $\Delta \geq \mathcal{O}(10^9)$ at low error rates.

¹ Machine epsilon, defined as the smallest ϵ such that $1 + \epsilon > 1$, is $\mathcal{O}(10^{-16})$ for all numerical data

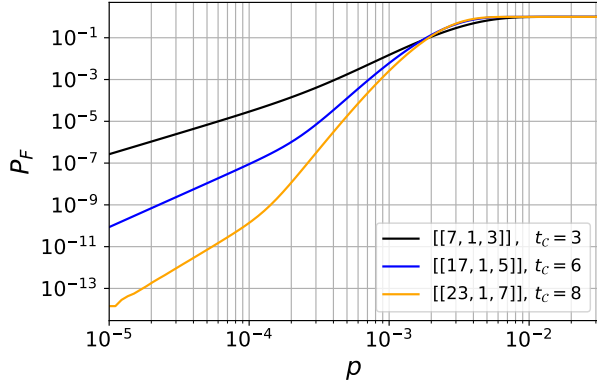


FIG. 4. Failure probability (25) for $L = 127$ Steane, color and Golay logical qubits plotted versus physical error rate assuming independent, Bernoulli error sources.

2. Noisy Syndrome Encoding

Faulty two-qubit gates and measurement errors are likely to dominate in any quantum processor. This is certainly the case in the current generation of devices that exhibit two-qubit gate error rates often two orders of magnitude greater than errors from faulty single qubit rotations or random errors occurring while qubits are idle. Continuing within the source coding framework, since two-qubit gates provide the syndrome encoding mechanism, we view two-qubit errors as *encoding* errors, assumed to be generated by a Bernoulli source \mathcal{E} with probability p_e . To simplify matters, assume that \mathcal{E} affects a (classical) bit-flip in the syndrome measurement outcome and does not leave additional errors in the data qubits.

The product code construction can be adapted to identify errors in the measured syndromes by using a higher distance classical code and encoding fewer logical qubits. To this end, recall that the generator matrix \mathbf{G} of a classical $[n, k, d]$ code maps a *message* to a *codeword* by appending the message to its syndrome. For $\mathbf{G} = [\mathbf{A} \mid \mathbf{I}_k]$ in systematic form, a message vector \mathbf{m} is encoded as

$$\mathbf{m}\mathbf{G} = [\mathbf{m}\mathbf{A} \mid \mathbf{m}] \quad (29)$$

We exploit the defining properties of classical codes, namely

$$wt(\mathbf{m}\mathbf{G} \oplus \mathbf{m}'\mathbf{G}) \geq d \quad (30)$$

for $\mathbf{m} \neq \mathbf{m}'$ and an error corrupted codeword $\mathbf{m}\mathbf{G} \oplus \mathbf{z}$ with $wt(\mathbf{z}) \leq \lfloor \frac{d-1}{2} \rfloor = t$ is closer to $\mathbf{m}\mathbf{G}$ (in Hamming distance) than it is to any other codeword.

Let $t_{src} < t_c$ denote the maximum number of source errors and $\mathbf{E} \neq \mathbf{E}'$ be $n \times M$ error patterns such that $wt_c(\mathbf{E}), wt_c(\mathbf{E}') \leq t_{src}$. As elements of \mathbb{E} (defined by setting $t_c = t_{src}$), the \mathcal{Q} -syndromes $\Sigma = H_{\mathcal{Q}}\mathbf{E} \neq H_{\mathcal{Q}}\mathbf{E}' = \Sigma'$ and, in particular, at least one row of Σ differs from at least one row of Σ' . Let Σ_{i*} and $\Sigma'_{i'*}$ denote the unequal

rows of Σ and Σ' , respectively. The key is to view the rows of Σ as “hyper-messages” encoded in a manner analogous to the classical case (29), but with the important distinction that in the quantum setting the messages are never transmitted, only their syndromes are measured and used by the decoder.

Express the parity-check matrix of \mathcal{C} in systematic form $[\mathbf{I}_R \mid \mathbf{A}^{\top}]$. For this construction, $H_{\mathcal{C}} = \mathbf{A}^{\top}$ must be used (thereby reducing the size of the block of logical qubits). By (30), we have

$$wt([\Sigma_{i*}\mathbf{A} \mid \Sigma_{i*}] \oplus [\Sigma'_{i'*}\mathbf{A} \mid \Sigma'_{i'*}]) \geq d_c \quad (31)$$

and, since Hamming distance is defined component-wise,

$$wt(\Sigma_{i*}\mathbf{A} \oplus \Sigma'_{i'*}\mathbf{A}) \geq d_c - wt(\Sigma_{i*} \oplus \Sigma'_{i'*}) \quad (32)$$

Let $\Xi_{i*} = \Sigma_{i*}\mathbf{A}$ denote the i -th row of the measured syndrome Ξ corresponding to Σ_{i*} . Similarly, let $\Xi'_{i'*} = \Sigma'_{i'*}\mathbf{A}$. By assumption $wt(\Sigma_{i*} \oplus \Sigma'_{i'*}) \leq 2t_{src}$ and (32) may be written as

$$wt(\Xi_{i*} \oplus \Xi'_{i'*}) \geq d_c - 2t_{src} \quad (33)$$

showing that unequal rows of the measured syndromes maintain the distance of the code less twice the maximum number of source errors. Since $wt(\Xi \oplus \Xi') \geq wt(\Xi_{i*} \oplus \Xi'_{i'*})$, the full product syndromes inherit this distance

$$wt(\Xi \oplus \Xi') \geq d_c - 2t_{src} \quad (34)$$

and, by the second property of classical codes, an erroneous measurement $\Xi \oplus \mathbf{T}$, for an error pattern $\mathbf{T} \sim \mathcal{E}$ such that

$$wt(\mathbf{T}) \leq \left\lfloor \frac{d_c - 2t_{src} - 1}{2} \right\rfloor = t_c - t_{src} \quad (35)$$

is closer to Ξ than any other Ξ' . Note that the weight of \mathbf{T} can occur anywhere in the product syndrome Ξ .

Once the expected maximum number of source errors t_{src} is determined, decoding for the error class

$$\bar{\mathbb{E}} = \mathbb{E} \cup \{\mathbf{T} \mid wt(\mathbf{T}) \leq t_c - t_{src}\} \quad (36)$$

is performed by nearest (in Hamming distance) neighbor search on the keys (product syndromes) of the lookup table for $\bar{\mathbb{E}}$. This *minimum distance decoder* turns out to be the maximum-likelihood decoder for independent Bernoulli error sources [28]. Moreover, there are a number of classical data structures and algorithms that efficiently perform minimum distance search in metric spaces by exploiting the triangle quality, such as a BK-tree [29], that can be employed for minimum distance decoding with a lookup table.

Assuming i.i.d two-qubit errors, the probability of an encoding error in a syndrome qubit scales with the number of two-qubit gates coupling to it. Thus the weight (or density) of a stabilizer $h_r \otimes s_i$, denoted $\delta_{ir} = wt(h_r \otimes s_i)$, is the relevant quantity in computing the failure probability due to encoding errors. Since an even number of

two-qubit errors in a syndrome qubit is self-correcting, the (i, r) -th syndrome measurement is given by the series

$$P_{ir} = \sum_{a \in O} \binom{\delta_{ir}}{a} p_e^a (1 - p_e)^{\delta - a} \quad (37)$$

where $O = \{1, 3, \dots, \delta\}$ is the set of odds less than (or equal to) δ_{ri} and the probability of an uncorrectable measurement error $P(\mathbf{T} > t_c - t_{src})$ follows a Poisson binomial distribution with probabilities $\{P_{ir}\}$.

3. Error Detection and Localization

Recall that error patterns \mathbf{D} such that $wt(\mathbf{D}_{*\ell}) < d_Q$ trigger non-zero \mathcal{Q} -syndromes and are detectable. With a syndrome decoder constructed from H_C only, a localization method can be devised for the set of error patterns

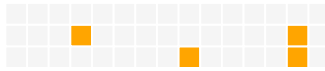
$$\mathbb{D} = \left\{ \mathbf{D} \in \{\mathbf{X}, \mathbf{Z}\} \mid wt(\mathbf{D}_{*\ell}) < d_Q, wt_c(\mathbf{D}) \leq t_c \right\} \quad (38)$$

Since \mathbb{D} contains detectable error patterns beyond the correction radius for \mathcal{Q} , there exist error patterns $\mathbf{D} \neq \mathbf{D}'$ with identical product syndromes $\Xi = \Xi'$, and the unambiguous lookup table decoder cannot be directly applied here. However, detectability of logical qubit errors is sufficient for localization since the \mathcal{Q} -syndrome $H_Q \mathbf{D}$ has $wt_c(\mathbf{D})$ non-zero columns, and the support (non-zero indices) of the rows of $H_Q \mathbf{D}$ are contained in the index set $\mathbb{L} \subset \{1, 2, \dots, L\}$ of logical qubits with errors.

For example, consider a block of 15 Steane logical qubits cross coded with a 3-error correcting BCH code $\mathcal{C} \sim [15, 5, 7]$. Under the action of H_Q , the weight-5 error pattern



with $\mathbb{L} = \{4, 9, 14\}$ transforms to the \mathcal{Q} -syndrome



Again, we interpret the rows of $H_Q \mathbf{D}$ as messages compressed by H_C , and provided $wt_c(\mathbf{D}) \leq t_C$, the rows of Ξ are leaders of their cosets under H_C . A decoder designed for H_C (such as a lookup table) applied to each row of the measured product syndrome can unambiguously recover a subset of the logical qubits with errors.

Returning to the example, decoding the rows of the product syndrome $H_Q \mathbf{D} H_C^\top$ illustrated as

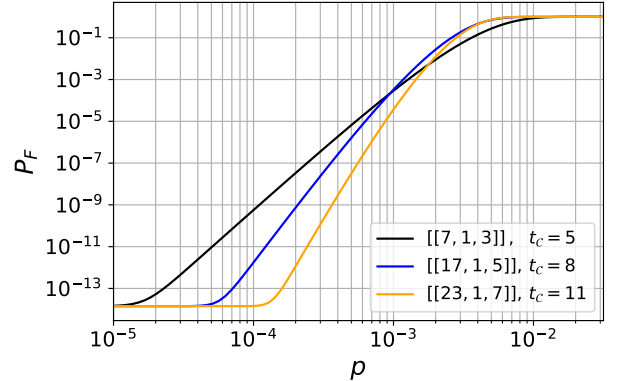


FIG. 5. Localization failure probability for Steane, color and Golay logical qubits plotted versus physical error rate assuming independent, Bernoulli error sources.

yields the row index sets $\{\{\}, \{4, 14\}, \{9, 14\}\}$, from which we conclude that logical qubits $\{4, 9, 14\}$ contain errors. To complete the error correction cycle using the localization results, syndrome extraction using H_Q from each of the logical qubits in \mathbb{L} determines which data qubits contain errors.

We can exploit source-channel duality to identify errors in the syndrome measurements by encoding M logical qubits and using a channel decoder designed for $\mathcal{C} \sim [L, M, d_C]$. Simply append a length- M zero message to a row of the measured product syndrome $\Xi_{i*} \oplus \mathbf{T}_i$ to form the codeword $[\Xi_{i*} \oplus \mathbf{T}_i \mid \mathbf{0}]$ and use a classical channel decoder. For \mathcal{C} in the BCH family, an algebraic decoder such as the Berlekamp-Massey algorithm [30] will correctly identify errors in the data qubits by interpreting the zero message as erroneous and return the length- M reconstruction of the “message” corresponding to Ξ_{i*} . As a channel decoder, protection against errors extends to the syndrome provided that the total number of errors $wt([\mathbf{T}_i \mid \mathbb{L}]) \leq t_c$.

Logical qubit localization holds advantages over error correction since $\mathbb{D} \supset \mathbb{E}$, and we may use the much lower probabilities $P(wt(\mathbf{D}_{*\ell}) \geq d_Q)$ (see Table I) in estimating the failure probability P_F . FIG. 5 shows the probability of a localization error in $L = 127$ Steane, color, and Golay logical qubits versus physical error rate. For each quantum code, a single t_c -BCH code satisfying $P(wt_c(\mathbf{E}) > t_c) \sim \mathcal{O}(LP(wt(\mathbf{E}_{*\ell}) \geq d_Q))$ was chosen assuming $p = 10^{-4}$.

E. Product Channel Coding

A final construction completes a Shannon coding theory for the quantum register by channel coding the compressed source syndrome Ξ . That is, we treat Ξ as a message to be encoded by a classical error correcting code and sent over a noisy channel, such as a quantum bus or

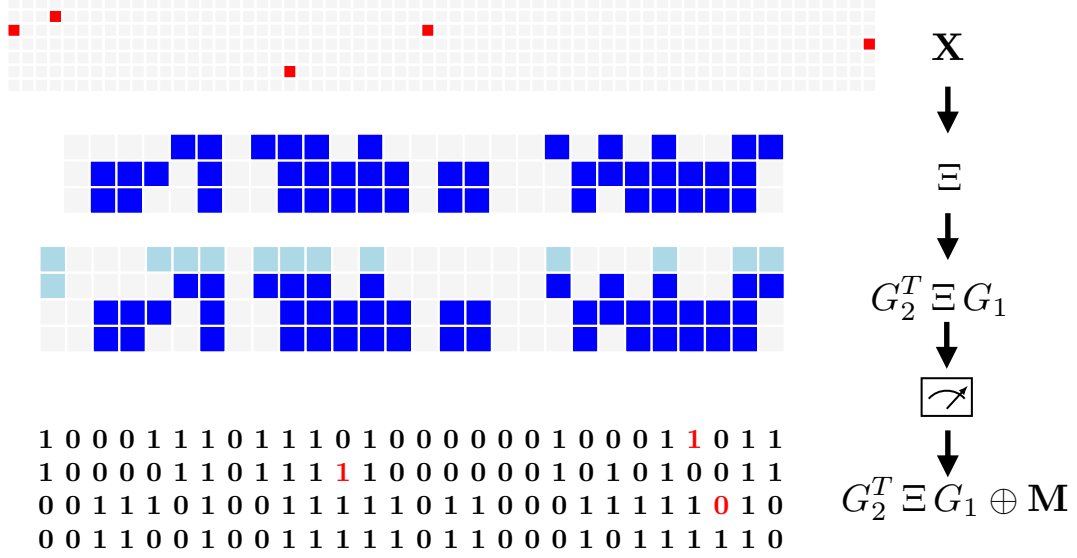


FIG. 6. Illustration of quantum error source and channel coding with the Steane quantum code, a [63, 36, 11] BCH classical source code, and a single parity-check product channel code. Identity operators in the rectangular representation are white and non-identity are colored. From top: a weight-5 error pattern \mathbf{X} on 63 Steane logical qubits is compressed with a 5-error correcting BCH code to a 3×27 source syndrome $\Xi = H_Q^T \mathbf{X} H_C^T$ and coded for the measurement channel with single-parity-check codes \mathbf{G}_1 and \mathbf{G}_2 . Bit-flips in the measurement outcomes due to \mathbf{M} are shown in red.

measurement apparatus. To this end, let $\mathcal{C}_1 \sim [n_1, R, d_1]$ and $\mathcal{C}_2 \sim [n_2, (n - k), d_2]$ be classical codes and consider the binary matrix

$$\mathbf{G}_1^T H_C \otimes \mathbf{G}_2^T H_Q \quad (39)$$

with systematic generator matrices $\mathbf{G}_1 = [\mathbf{A}_1 \mid \mathbf{I}_R]$, $\mathbf{G}_2 = [\mathbf{A}_2 \mid \mathbf{I}_{(n-k)}]$ of \mathcal{C}_1 and \mathcal{C}_2 , respectively. The rows of $\mathbf{G}_2^T H_Q$ are (modulo 2) linear combinations of the rows of H_Q and hence in \mathcal{S} . As the Kronecker product of any binary matrix with a quantum parity-check matrix is in the product stabilizer group, we conclude that the rows of (39) are in \mathcal{G} and therefore suitable for quantum error syndrome extraction. For an error pattern \mathbf{E} , source-channel coding may be expressed as

$$\mathbf{G}_2^T H_Q \mathbf{E} H_C^T \mathbf{G}_1 = \mathbf{G}_2^T \Xi \mathbf{G}_1 \quad (40)$$

which may be arranged as the matrix

$$\begin{bmatrix} \mathbf{A}_2^T \Xi \mathbf{A}_1 & \mathbf{A}_2^T \Xi \\ \Xi \mathbf{A}_1 & \Xi \end{bmatrix} \quad (41)$$

where the submatrices $[\mathbf{A}_2^T \Xi \mid \Xi]^T \in \mathcal{C}_2$ and $[\Xi \mathbf{A}_1 \mid \Xi] \in \mathcal{C}_1$. The remaining component $\mathbf{A}_2^T \Xi \mathbf{A}_1$ is often referred to as *checks on checks* and is unique to product codes. The resulting product code has parameters $[n_1 n_2, R(n - k), d_1 d_2]$. This matrix is in the form of a (direct) product code as originally proposed by Elias [31] and recognized as the Kronecker product by Slepian [32]. The use of a classical error correcting code to identify

measurement errors in a single logical qubit was first proposed by Zalka [33] using a single-parity-check code and more generally, with an arbitrary classical error correcting code as described in Gottesman [11] and attributed to unpublished work of Evslin, Kakade and Preskill therein. In our construction, by virtue of the Kronecker product, this procedure is extended from a single logical qubit to a block of logical qubits.

The full source-channel product coding construction is illustrated in FIG. 6. Analogous to the classical case, source and channel coding are depicted separately, though these operations happen concurrently in the quantum setting. Under the action of $H_C \otimes H_Q^T$, the error pattern \mathbf{X} is compressed to source syndrome Ξ (blue). Single-parity-check codes \mathcal{C}_i with $\mathbf{A}_i = [1, 1, \dots, 1]^T$ compute parity-checks across each row and column of Ξ (light blue). Product channel coding adds the check-on-check bit in the top left corner (light blue) and the source syndrome itself is sent through the measurement channel. Measurements corrupted by an error pattern \mathbf{M} flip bits in the observed binary outcomes (red).

Decoding the channel code may be performed with a classical decoder to recover the noise corrupted source syndrome Ξ , which may be queried against a lookup table constructed from the pair $(\mathcal{C}, \mathcal{Q})$. Shannon's second theorem [14] characterizes the capacity of a discrete, memoryless channel as the limiting rate at which a message can be sent reliably through a noisy channel in terms of the maximum mutual information between the source (compressed error sources Ξ) and channel out-

puts (channel syndrome measurements $\mathbf{G}_2^\top \Xi \mathbf{G}_1 \oplus \mathbf{M}$). For a binary symmetric measurement channel parameterized by p_m , the channel capacity is given by $1 - H_2(p_m)$. For the linear product codes considered here, Shannons noisy-channel coding theorem yields the bound $R(n - k)/n_1 n_2 < 1 - H_2(p_m)$.

III. DISCUSSION

A. Fault-Tolerance

Our construction violates the first law of fault-tolerant quantum error correction (FTQEC): *never use a syndrome qubit more than once* [34, 35]. Adherence to this law prevents an error in the preparation (or reuse) of a syndrome qubit from propagating to a high weight, undetectable error pattern in a logical qubit. As proposed by Shor [34] and Steane [36], syndrome extraction may be made fault-tolerant by preparing blocks of syndrome qubits in an entangled state, coupling to the entangled block, and performing a parity measurement on the entangled block to obtain the syndrome bit. In this way, each data qubit interacts with a single syndrome qubit, preventing a cascade of errors from subsequent couplings. At the cost of extra syndrome qubits, errors in the syndrome qubits only propagate to low weight errors in the logical qubits which may then be caught and corrected in future rounds of error correction. Central to our scheme, however, is the coupling of *multiple* logical qubits to the *same* syndrome qubit potentially exacerbating the propagation of errors.

A full fault-tolerant analysis is beyond the scope of this work, but we consider some key issues here. Referring to the circuit in Fig. 1 and assuming that the syndrome qubits are prepared in the $|0\rangle$ state, a Y -type error in the first syndrome qubit will propagate to a weight-2 Z -type error in the logical qubits $|\psi_1\rangle$, $|\psi_2\rangle$ and $|\psi_3\rangle$. However, fault-tolerance may be recovered in the product coding scheme by adapting Shor's method [34] as illustrated in Fig. 7. This circuit first prepares Bell states $|\alpha_i\rangle = (|00\rangle + |11\rangle)/\sqrt{2}$ (not shown in Fig. 7) and couples each data qubit to a logical qubit in a Bell state as prescribed by the classical and quantum error correcting codes used in the construction (i.e. $H_C \otimes H_Q$). For example, in Fig. 7, the first data qubits in logical qubits $|\psi_1\rangle$, $|\psi_2\rangle$ and $|\psi_3\rangle$ are coupled to the first qubit in $|\alpha_1\rangle$, and the second data qubits in logical qubits $|\psi_1\rangle$, $|\psi_2\rangle$ and $|\psi_3\rangle$ are coupled to the second qubit in $|\alpha_1\rangle$, completing the couplings specified by the first row of $\mathbf{A}^\top \otimes [110]$. The remaining rows of $\mathbf{A}^\top \otimes [110]$ are implemented similarly. As before, each logical qubit interacts with multiple Bell states, but coupling the qubits in this fashion ensures that a single fault in a Bell state propagates to a single error in the logical qubits to which it is coupled, and thus retains the fault-tolerance property. To be fully fault-tolerant, one must repeat the measurement a number of times until

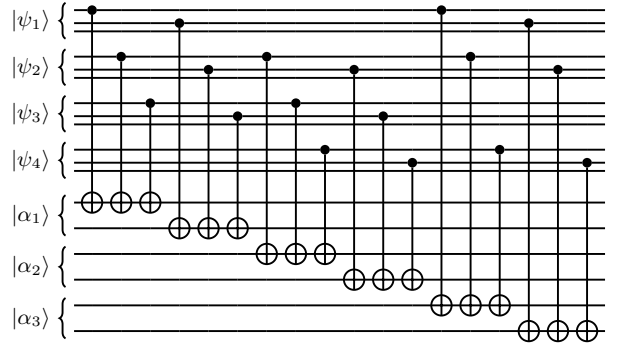


FIG. 7. Fault-tolerant implementation of the stabilizer circuit of Fig. 1. Ancilla blocks $|\alpha_i\rangle$ are prepared in Bell states. Fault-tolerant syndrome extraction is performed by coupling each data qubit in a logical qubit ($|\psi_j\rangle$) to a separate ancilla qubit. Each Bell state ancilla block is coupled to multiple logical qubits, but a single error in an ancilla qubit propagates to a weight-1 error in each logical qubit to which it is coupled.

convergence as described in [34].

To account for Shor style fault-tolerant syndrome extraction, the qubit overhead rates $R(n - k)$ in Fig. 3 are scaled by the weights of the stabilizers, which for the Steane code is 4 (see Appendix A 2 a), yielding an overhead rate of $4R(n - k)$. The color code has 7 weight-4 stabilizers and a weight-8 stabilizer for each error type (see Appendix A 2 b), and an overhead rate of $4R(n - k - 2) + 16R$ when syndrome extraction is performed fault-tolerantly.

B. Ancillary Processes

The product code construction applies to quantum processes that employ non-destructive measurements from data qubits to ancillary qubits as a computational or post-selection primitive. So-called *ancilla factories* are one such application in which multiple-qubit entangled states (e.g. cat states, quantum codewords) are constructed and verified by measuring Pauli operators on the data qubits by coupling to ancillary qubits. Based on the measurement results of the ancillary qubits, the entangled state is accepted or discarded. The basic principle proposed here—error extraction from blocks of entangled states and collective inference—may be used to verify multiple entangled states simultaneously. Moreover, for this type of post-selection task we may use the detection and localization method as described previously, since any failure of a verification test leads to destruction of the state undergoing verification—which qubit in the entangled state containing the error is not important.

Consider, for example, the verification of n -qubit cat states of the form $(|00\cdots 0\rangle + |11\cdots 1\rangle)/\sqrt{2}$. As illustrated by the 2-qubit cat (or Bell) states in Fig. 7, these states facilitate fault-tolerant syndrome extraction. More generally, n -qubit cat states transformed via transversal

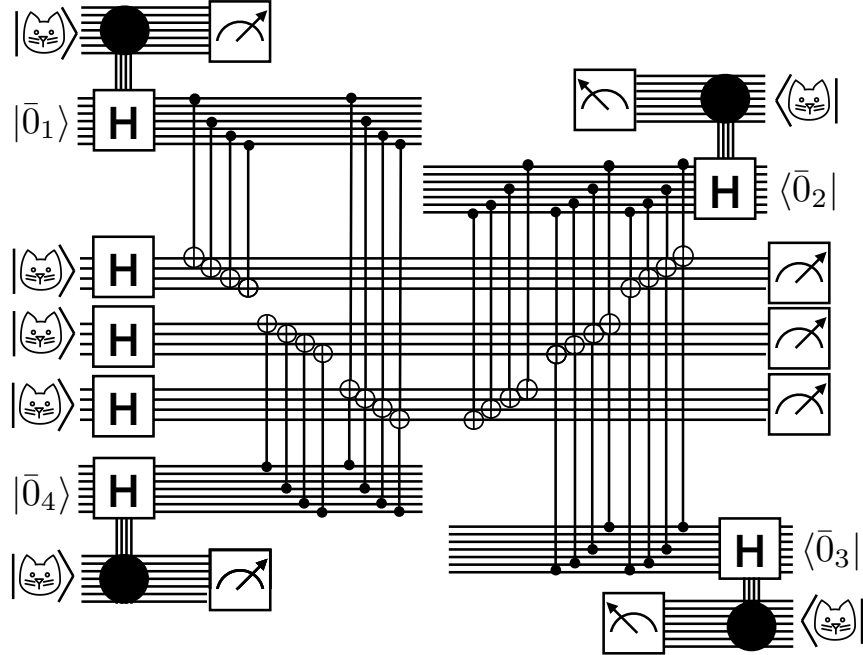


FIG. 8. Fault-tolerant encoded magic state factory. Cat states and Steane zero codewords are prepared and verified against weight-2 errors by ancilla factories (not shown). Cat states are used to prepare a magic state $\pm|H\rangle$ by fault-tolerantly measuring a transversal Hadamard. CNOT gates with common targets are overlaid for clarity. Error detection and localization is performed fault-tolerantly with additional cat states and Steane syndrome extraction, shown here by product coding with $\mathbf{A}^\top \otimes [1001011]$. Any magic states found with errors are discarded. The process iterates by cycling through the remaining Steane stabilizers with a shortened classical parity-check matrix to couple the reduced number of magic states.

Hadamard gates create even-parity states for use in fault-tolerant syndrome extraction for any quantum code. Cat states are verified by performing CNOT gates from the first and last qubits in the cat state to an ancilla qubit initialized as $|0\rangle$. A non-zero measurement of the ancilla indicates that the cat state contains a weight-2 error [35], and is therefore not suitable for fault-tolerant operations and discarded. The n -qubit cat state verification circuit is represented by the binary vector $V = [10 \cdots 01]$, and an ancilla factory constructing multiple cat states may be verified by error localization and post-selection based on source coding with $H_C \otimes V$. More generally, for example in the verification of quantum codeword encoding [35], V is a matrix composed of check operators arranged as rows.

Magic states are key resource states in FTQEC as they complete the Clifford group of transformations to form a universal set of quantum logic operations [37]. The magic state $|H\rangle = (|0\rangle + e^{i\pi/4}|1\rangle)/\sqrt{2}$ can be used to simulate a logical T gate on encoded qubits, and the set $\text{Clifford} + T$ is known to be universal for quantum computation. Imperfect magic states can be iteratively improved by state distillation [37], however distillation techniques are not inherently fault-tolerant. Alternatively, an *encoded* magic state can be constructed fault-tolerantly and used directly to simulate logical T gates and achieve universality [38].

A fault-tolerant encoded magic state factory can be

built by combining the methods proposed in this work as illustrated in Fig. 8. The parity-check matrix \mathbf{A}^\top from the $[7, 4, 3]$ Hamming code (11) multiplexes error detection from 4 encoded magic states. The factory consumes 7-qubit cat states and Steane encoded zero states $|\bar{0}_j\rangle$, $1 \leq j \leq 4$. These states are the outputs of ancilla factories producing cat states and quantum codewords verified against weight-2 errors as described above. Ancilla blocks prepared in cat states fault-tolerantly measure the Hadamard operator and project the Steane zero codewords $|\bar{0}_j\rangle$ onto a magic state $\pm|H\rangle$. The sign of the projected magic state is determined by a measurement of the cat state. Verified 4-qubit cat states are consumed for fault-tolerant error detection and localization based on the stabilizers of the Steane code. Transversal Hadamards first transform the 4-qubit cat states to an even parity state to carry out Shor style fault-tolerant syndrome extraction. The CNOT gates in Fig. 8 couple the errors to the ancilla blocks fault-tolerantly implementing the source code $\mathbf{A}^\top \otimes [1001011]$, corresponding to the Steane code stabilizer $Z_1Z_4Z_6Z_7$. Errors in the encoded magic states are localized by decoding the rows of Ξ as described previously and those states are discarded. The process iterates by cycling through the remaining Steane code stabilizers, perhaps with a reduced number of magic states and discarding encoded magic states found with errors. To accommodate fewer encoded magic states, the classical code may be shortened by re-

moving columns from H_C .

C. Asymmetric and Correlated Error Models

Our source coding constructions employed a single classical code for compression of X and Z error sources. With CSS codes, as investigated here, one can choose separate codes for correcting X and Z errors to reflect asymmetry in the error rates. Dephasing is likely to dominate in qubits with a Z -type energy splitting, thus motivating interest in error correction protocols designed for asymmetric error models. With an independent error model, the achievable compression rate of an encoding scheme with separate classical codes for each error type (e.g. \mathcal{C}_X and \mathcal{C}_Z) is asymptotically limited by $H(\mathcal{X}) + H(\mathcal{Z})$ by Shannon's theorem.

A single data qubit may exhibit correlations between dephasing and bit-flip errors as observed in the paradigmatic depolarizing noise model [39]. Coding for correlated classical sources is characterized by the Slepian-Wolf theorem [40]: if a model of the correlations is known, Slepian and Wolf established the joint entropy $H(\mathcal{X}, \mathcal{Z}) \leq H(\mathcal{X}) + H(\mathcal{Z})$ as the achievable rate with separate coding for \mathcal{X} and \mathcal{Z} . Remarkably, knowledge of \mathcal{X} is not needed to compress \mathcal{Z} (and vice versa) but joint decoding $\{\mathcal{X}, \mathcal{Z}\}$ with the aid of a model can achieve the joint entropy rate.

Given our assertion that syndrome extraction performs *classical* data compression, by Slepian-Wolf, separate encodings for phase and bit-flip errors are possible (using, for example, the implementation described in [41]), provided a model of the correlated errors is known. Quantum noise spectroscopy protocols have recently been extended to estimate multiple-axis noise correlations from experimental data [42], perhaps providing a path toward accurate correlated error models that could be used in

this setting.

IV. CONCLUSION

In this work, we have proposed a versatile and efficient product code construction for syndrome extraction from the encoded quantum register. The construction connects Shannon's coding theorems and associated bounds to the overhead rates of QEC and other quantum post-selection tasks. To demonstrate our method, we have investigated the BCH family of codes and lookup table decoders for unambiguous (lossless) compression and error reconstruction. The size of the lookup table is exponential in the number of allowable errors (t_C) and combinatorial in problem size (L), limiting the ultimate utility of a lookup table decoder. Nonetheless, a proof of concept design reaching quantum advantage sized problems and circuits in the low noise regime was presented. For BCH codes, the Berlekamp-Massey algorithm may be used to locate logical qubits with errors even in the presence of syndrome noise.

Improvements in decoding and different classical encodings will likely accommodate higher error rates. In particular, the density of the classical code drives the tolerable two-qubit error rate by the dependence on the weight of the product stabilizers in the probability of a decoding error. Algebraic codes, such as the BCH family, are *high density* codes, comprised of high weight parity-check constraints. The construction with a classical *low-density parity-check* (LDPC) code [43] would therefore achieve a better compression ratio by reducing the number of two-qubit gates needed for syndrome extraction. A number of deterministic and random LDPC constructions, as well as probabilistic belief-propagation decoders [44] are known to achieve excellent performance in practice in the classical setting. Thus, the use of LDPC codes as the classical code in our construction and iterative belief-propagation or neural based decoders, are topics of great interest.

[1] Stephen Jordan. Quantum algorithm zoo <https://quantumalgorithmzoo.org>.

[2] D. Aharonov and M. Ben-Or. Fault-tolerant quantum computation with constant error. In *Proceedings of the Twenty-Ninth Annual ACM Symposium on Theory of Computing*, STOC '97, pages 176–188, New York, NY, USA, 1997. Association for Computing Machinery.

[3] Emanuel Knill and Raymond Laflamme. Concatenated quantum codes. *arXiv preprint quant-ph/9608012*, 1996.

[4] Markus Reiher, Nathan Wiebe, Krysta M Svore, Dave Wecker, and Matthias Troyer. Elucidating reaction mechanisms on quantum computers. *Proceedings of the National Academy of Sciences*, 114(29):7555–7560, 2017.

[5] Ryan Babbush, Craig Gidney, Dominic W Berry, Nathan Wiebe, Jarrod McClean, Alexandru Paler, Austin Fowler, and Hartmut Neven. Encoding electronic spectra in quantum circuits with linear t complexity. *Physical Review X*, 8(4):041015, 2018.

[6] Craig Gidney and Martin Ekerå. How to factor 2048 bit RSA integers in 8 hours using 20 million noisy qubits. *arXiv preprint arXiv:1905.09749*, 2019.

[7] Charles H. Bennett, David P. DiVincenzo, John A. Smolin, and William K. Wootters. Mixed-state entanglement and quantum error correction. *Phys. Rev. A*, 54:3824–3851, Nov 1996.

[8] Seth Lloyd. Capacity of the noisy quantum channel. *Physical Review A*, 55(3):1613, 1997.

[9] Peter Shor. The quantum channel capacity and coherent information. Lecture notes, MSRI Workshop on Quantum Computation, 2002.

[10] Igor Devetak. The private classical capacity and quantum capacity of a quantum channel. *IEEE Transactions on*

Information Theory, 51(1):44–55, 2005.

[11] Daniel Gottesman. *Stabilizer codes and quantum error correction*. PhD thesis, California Institute of Technology, 1997.

[12] Mark M Wilde. *Quantum information theory*. Cambridge University Press, 2013.

[13] A Robert Calderbank, Eric M Rains, Peter W Shor, and Neil JA Sloane. Quantum error correction and orthogonal geometry. *Physical Review Letters*, 78(3):405, 1997.

[14] Claude Shannon. A mathematical theory of communication. *Bell System Technical Journal*, 27(3):379–423, 1948.

[15] ER Berlekamp, RJ McEliece, and HCA Van Tilborg. On the inherent Intractability of certain coding problems. *Transaction on Information Theory*, 24:383–386, 1978.

[16] Min-Hsiu Hsieh and François Le Gall. NP-hardness of decoding quantum error-correction codes. *Physical Review A*, 83(5):052331, 2011.

[17] Pavithran Iyer and David Poulin. Hardness of decoding quantum stabilizer codes. *IEEE Transactions on Information Theory*, 61(9):5209–5223, 2015.

[18] Eric Dennis, Alexei Kitaev, Andrew Landahl, and John Preskill. Topological quantum memory. *Journal of Mathematical Physics*, 43(9):4452–4505, 2002.

[19] Austin G. Fowler, Adam C. Whiteside, and Lloyd C. L. Hollenberg. Towards practical classical processing for the surface code. *Phys. Rev. Lett.*, 108:180501, May 2012.

[20] Ye-Hua Liu and David Poulin. Neural belief-propagation decoders for quantum error-correcting codes. *Phys. Rev. Lett.*, 122:200501, May 2019.

[21] Markus Grassl and Martin Rötteler. Quantum block and convolutional codes from self-orthogonal product codes. In *Proceedings. International Symposium on Information Theory, 2005. ISIT 2005.*, pages 1018–1022. IEEE, 2005.

[22] Jihao Fan, Yonghui Li, Min-Hsiu Hsieh, and Hanwu Chen. On quantum tensor product codes. *Quantum Info. Comput.*, 17(13–14):1105–1122, November 2017.

[23] J Wolf. On codes derivable from the tensor product of check matrices. *IEEE Transactions on Information Theory*, 11(2):281–284, 1965.

[24] Hideki Imai and Hiroshi Fujiya. Generalized tensor product codes. *IEEE Transactions on Information Theory*, 27(2):181–187, 1981.

[25] Jean-Pierre Tillich and Gilles Zémor. Quantum LDPC codes with positive rate and minimum distance proportional to the square root of the blocklength. *IEEE Transactions on Information Theory*, 60(2):1193–1202, 2013.

[26] A Robert Calderbank and Peter W Shor. Good quantum error-correcting codes exist. *Physical Review A*, 54(2):1098, 1996.

[27] Andrew Steane. Multiple-particle interference and quantum error correction. *Proceedings of the Royal Society of London. Series A: Mathematical, Physical and Engineering Sciences*, 452(1954):2551–2577, 1996.

[28] Peterson and Weldon. *Error-correcting codes*. MIT press, 1972.

[29] Walter A. Burkhard and Robert M. Keller. Some approaches to best-match file searching. *Communications of the ACM*, 16(4):230–236, 1973.

[30] Elwyn Berlekamp. *Algebraic coding theory*. World Scientific, 1968.

[31] Peter Elias. Error-free coding. *Transactions of the IRE Professional Group on Information Theory*, 4(4):29–37, 1954.

[32] David Slepian. Some further theory of group codes. *Bell System Technical Journal*, 39(5):1219–1252, 1960.

[33] Christof Zalka. Threshold estimate for fault tolerant quantum computation. *arXiv preprint quant-ph/9612028*, 1996.

[34] Peter W Shor. Fault-tolerant quantum computation. In *Proceedings of 37th Conference on Foundations of Computer Science*, pages 56–65. IEEE, 1996.

[35] John Preskill. Reliable quantum computers. *Proceedings of the Royal Society of London. Series A: Mathematical, Physical and Engineering Sciences*, 454(1969):385–410, 1998.

[36] Andrew M Steane. Efficient fault-tolerant quantum computing. *Nature*, 399(6732):124, 1999.

[37] Sergey Bravyi and Alexei Kitaev. Universal quantum computation with ideal clifford gates and noisy ancillas. *Phys. Rev. A*, 71:022316, Feb 2005.

[38] Panos Aliferis, Daniel Gottesman, and John Preskill. Quantum accuracy threshold for concatenated distance-3 codes. *Quantum Info. Comput.*, 6(2):97–165, March 2006.

[39] Nicolas Delfosse and Jean-Pierre Tillich. A decoding algorithm for css codes using the x/z correlations. In *2014 IEEE International Symposium on Information Theory*, pages 1071–1075. IEEE, 2014.

[40] David Slepian and Jack Wolf. Noiseless coding of correlated information sources. *IEEE Transactions on information Theory*, 19(4):471–480, 1973.

[41] Aaron Wyner. Recent results in the shannon theory. *IEEE Transactions on information Theory*, 20(1):2–10, 1974.

[42] Gerardo A Paz-Silva, Leigh M Norris, Félix Beaudoin, and Lorenza Viola. Extending comb-based spectral estimation to multiaxis quantum noise. *Physical Review A*, 100(4):042334, 2019.

[43] Robert Gallager. Low-density parity-check codes. *IRE Transactions on information theory*, 8(1):21–28, 1962.

[44] Sarah J Johnson. *Iterative error correction: Turbo, low-density parity-check and repeat-accumulate codes*. Cambridge university press, 2010.

[45] Edwin Weiss. Compression and coding (corresp.). *IRE Transactions on Information Theory*, 8(3):256–257, 1962.

[46] H. Bombin and M. A. Martin-Delgado. Topological quantum distillation. *Phys. Rev. Lett.*, 97:180501, Oct 2006.

[47] H. Bombin. Topological subsystem codes. *Phys. Rev. A*, 81:032301, Mar 2010.

[48] Christopher Chamberland and Tomas Jochym-O’Connor. Error suppression via complementary gauge choices in reed-muller codes. *Quantum Science and Technology*, 2(3):035008, 2017.

Appendix A: Notation and background

1. Binary Linear Block Codes

Error correcting codes protect messages against errors incurred during transmission by adding redundant bits to the message. A code $\mathcal{C} \sim [n, k, d]$ is parameterized by the codeword length n , message length k , and code distance d . A binary, linear code \mathcal{C} forms a k -dimensional subspace of \mathbb{F}_2^n represented by k linearly independent generator codewords $\mathbf{g}_1, \mathbf{g}_3, \dots, \mathbf{g}_k$. Arranging the generators \mathbf{g}_i as rows of a $k \times n$ binary generator matrix \mathbf{G} , a binary message \mathbf{m} is mapped to a codeword by matrix multiplication $\mathbf{m}\mathbf{G}$. For binary codes, arithmetic is performed in \mathbb{F}_2^n , that is, modulo 2. The generator matrix may be expressed systematic form $\mathbf{G} = [\mathbf{A} \mid \mathbf{I}_k]$, where the $k \times (n - k)$ matrix \mathbf{A} defines a set of parity conditions that fix the redundant bits based on the message to obtain $\mathbf{m}\mathbf{G} = [\mathbf{m}\mathbf{A} \mid \mathbf{m}]$. Note that for a generator matrix in systematic form, the transmitted codeword contains the redundant part and the message itself. The Hamming weight $wt(\mathbf{v})$ of a binary vector \mathbf{v} is the number of its non-zero entries. A code's distance d is the defining parameter of the code since it specifies the minimum Hamming weight of all the codewords and the minimum Hamming distance, defined as the number of places where two binary vectors differ, between any two codewords. A distance d code is capable of correcting all error patterns within the error correction radius $t = \lfloor \frac{d-1}{2} \rfloor$, but unable to correct all error patterns with $t + 1$ errors.

An alternative description of a linear code is given by the $(n - k) \times n$ parity-check matrix \mathbf{H} defined as the orthogonal complement of \mathbf{G} in \mathbb{F}_2^n , namely $\mathbf{G}\mathbf{H}^\top = \mathbf{0}$, where $\mathbf{0}$ is a $k \times (n - k)$ zero matrix. Viewed as a linear mapping $\mathbf{H} : \mathbb{F}_2^n \rightarrow \mathbb{F}_2^{n-k}$, the parity-check matrix maps a length n vector to its $(n - k)$ length *syndrome*. By definition, \mathcal{C} is the kernel of \mathbf{H} and the quotient group $\mathbb{F}_2^n/\mathcal{C}$ is isomorphic to \mathbb{F}_2^{n-k} . The cosets of $\mathbb{F}_2^n/\mathcal{C}$ can be arranged in a table called the *standard array* and used for syndrome decoding. A *coset leader*, defined as a minimum weight n -vector in the coset, is chosen as the coset representative for each coset. A binary vector \mathbf{v} with $wt(\mathbf{v}) \leq t$ is always a unique coset leader since the weight of any other element of its coset $\mathbf{u} \in \mathbf{v} \oplus \mathcal{C}$, has weight $wt(\mathbf{u}) > t$ since $wt(\mathcal{C}) \geq d \geq 2t + 1$. By this property, t -error correcting codes can be used for data compression [45]: a length n binary vector is mapped to its $(n - k)$ length syndrome by \mathbf{H} . Provided the weight of the vector is not greater than t , this mapping is invertible and the syndrome uniquely identifies the original vector.

2. Quantum Error Correcting Codes

Let $\mathcal{P}_n = \langle \pm iI, X, Y, Z \rangle^{\otimes n}$ denote the Pauli group on n qubits, where $XZ = Y, XX = YY = ZZ = I$, and $XZ = -ZX$. The quotient group $\mathcal{P}_n / \{\pm iI\}$ is isomorphic to the binary vector space \mathbb{F}_2^{2n} . Binary vectors $u, v \in \{0, 1\}^{\oplus n} = \mathbb{F}_2^n$ define a general Pauli operator by $[u \mid v] := X(u)Z(v) = \bigotimes_{i=1}^n X_i^{u_i} \bigotimes_{i=1}^n Z_i^{v_i}$. Under the isomorphism, commutativity of two Pauli operators is determined by the identity

$$[u \mid v] \cdot [u' \mid v'] = (-1)^{u \cdot v' + u' \cdot v} [u' \mid v'] \cdot [u \mid v]$$

where $u \cdot v' = \oplus_i u_i v'_i$ is performed modulo 2. Thus, two Pauli operator commute if the *symplectic* inner product [13] $u \cdot v' + u' \cdot v$ vanishes.

Recall the properties of a distance d_Q quantum stabilizer code \mathcal{Q} encoding k logical qubits in n physical qubits capable of correcting $t = \lfloor (d_Q - 1)/2 \rfloor$ errors. Codewords are simultaneous +1 eigenstates of \mathcal{Q} 's stabilizer group \mathcal{S} , an abelian subgroup of the Pauli group such that $s|\psi\rangle = |\psi\rangle$ for any $|\psi\rangle \in \mathcal{Q}$ and $s \in \mathcal{S}$. In the stabilizer formalism, detectable errors anti-commute with \mathcal{S} and signal an error by observing a sign change in the stabilizer measurement outcomes. The CSS family of codes [26, 27] have stabilizer groups that are generated by distinct sets of either X or Z -type Pauli operators, so that $\mathcal{S} = \langle \mathcal{S}_X, \mathcal{S}_Z \rangle$ where $\mathcal{S}_X = \{X(\beta) : \beta \in S_X\}$, $\mathcal{S}_Z = \{Z(\alpha) : \alpha \in S_Z\}$ and S_X, S_Z are subspaces of \mathbb{F}_2^n . As linear subspaces, S_X and S_Z can be represented as matrices denoted, H_Q^X and H_Q^Z respectively, with the binary representation of the X and Z -type stabilizers arranged as rows. For CSS codes, the symplectic inner product reduces to the the modulo 2 inner product between X and Z -type Pauli operators. Error syndromes from X - and Z -type errors, $X(u), Z(v)$, are obtained by the commutation identities $Z(\alpha)X(u)|\psi\rangle = (-1)^{\alpha \cdot u} X(u)Z(\alpha)|\psi\rangle$ and $X(\beta)Z(v)|\psi\rangle = (-1)^{\beta \cdot v} Z(v)X(\beta)|\psi\rangle$. bit-flip and phase flip recovery operations are performed separately in CSS codes and its parity-check matrix has the block structure

$$H_Q = \begin{bmatrix} H_Q^Z & \mathbf{0} \\ \mathbf{0} & H_Q^X \end{bmatrix} \quad (\text{A1})$$

Under the isomorphism, error syndromes Σ_X and Σ_Z corresponding to Pauli errors $X(u)$ and $Z(v)$, respectively, can

s_X	s_Z
$X_1 X_4 X_6 X_7$	$Z_1 Z_4 Z_6 Z_7$
$X_2 X_4 X_5 X_7$	$Z_2 Z_4 Z_5 Z_7$
$X_3 X_4 X_5 X_6$	$Z_3 Z_4 Z_5 Z_6$

TABLE II. Generators of the stabilizer group of the Steane code

be formally obtained by modulo 2 matrix-vector multiplication

$$H_{\mathcal{Q}}^Z u = \Sigma_X \quad H_{\mathcal{Q}}^X v = \Sigma_Z \quad (\text{A2})$$

a. $[[7, 1, 3]]$ Steane code

The $[[7, 1, 3]]$ Steane code [27] protects against a single bit-flip or phase-flip on $n = 7$ physical qubits encoding $k = 1$ logical qubits. The Steane code is a CSS code constructed from the classical $[7, 4, 3]$ Hamming code and its dual. Pauli operators generating the stabilizer group are listed in Table II. The Steane code is a *dual-containing* code implying that $H_{\mathcal{Q}}^Z = H_{\mathcal{Q}}^X$. In the binary representation, with stabilizers arranged as rows, we have the quantum parity-check matrices

$$H_{\mathcal{Q}}^Z = H_{\mathcal{Q}}^X = \begin{bmatrix} 1 & 0 & 0 & 1 & 0 & 1 & 1 \\ 0 & 1 & 0 & 1 & 1 & 0 & 1 \\ 0 & 0 & 1 & 1 & 1 & 1 & 0 \end{bmatrix} \quad (\text{A3})$$

The Steane code has distance 3, and therefore weight-3 minimal weight generators of its normalizer group listed in Table III. The weight-4 normalizers are in the stabilizer, obtained by the product of all three generators of each error type in Table II.

η_X	η_Z
$X_1 X_2 X_3 X_4$	$Z_1 Z_2 Z_3 Z_4$
$X_2 X_3 X_5$	$Z_2 Z_3 Z_5$
$X_1 X_3 X_6$	$Z_1 Z_3 Z_6$
$X_1 X_2 X_7$	$Z_1 Z_2 Z_7$

TABLE III. Generators of the normalizer of the Steane code.

The Steane code is non-degenerate, meaning that correctable error patterns have a unique error syndrome. A lookup table pairing error syndromes to error patterns is shown in Table A 2 a in the case of bit-flips.

100	X_1
010	X_2
001	X_3
111	X_4
011	X_5
101	X_6
110	X_7

TABLE IV. bit-flip lookup table for the Steane code. Weight-1 bit-flips (second column) are indexed by the error syndrome determined from $H_{\mathcal{Q}}^Z$. Phase flip syndromes are identical but obtained independently by $H_{\mathcal{Q}}^X$ posing no ambiguity in the associated lookup table.

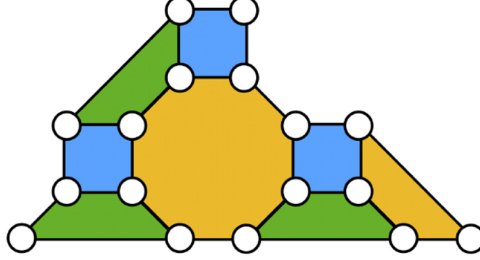


FIG. 9. Qubit layout for the $[[17, 1, 5]]$ color code (reproduced from [48]). Qubits are numbered left to right and top to bottom e.g. data qubits 13 - 17 are in the bottom row.

b. $[[17, 1, 5]]$ color code

Color codes [46, 47] are a class of topological QEC codes that allow for transversal implementations of the Clifford group. Here we present details for a distance 5 code capable of correcting error patterns of weight-2 ($t_Q = 2$) or less with parameters $[[17, 1, 5]]$. Color codes are CSS codes and therefore have stabilizer groups that partition into sets of Pauli- X or Z operators only. Syndrome measurements of Pauli- X (Z) are used to detect Z (X)-type errors. Figure 9 depicts the $[[17, 1, 5]]$ qubit. Each face defines a stabilizer of X and Z -type. In the binary representation, with stabilizer arranged as rows, we have the quantum parity-check matrix

$$H_Q = \begin{bmatrix} 1 & 1 & 1 & 1 & 0 & 0 & 0 & 0 & 0 & 0 & 0 & 0 & 0 & 0 & 0 & 0 & 0 \\ 1 & 0 & 1 & 0 & 1 & 1 & 0 & 0 & 0 & 0 & 0 & 0 & 0 & 0 & 0 & 0 & 0 \\ 0 & 0 & 0 & 0 & 1 & 1 & 0 & 0 & 1 & 1 & 0 & 0 & 0 & 0 & 0 & 0 & 0 \\ 0 & 0 & 0 & 0 & 0 & 0 & 1 & 1 & 0 & 0 & 1 & 1 & 0 & 0 & 0 & 0 & 0 \\ 0 & 0 & 0 & 0 & 0 & 0 & 0 & 0 & 1 & 1 & 0 & 0 & 1 & 1 & 0 & 0 & 0 \\ 0 & 0 & 0 & 0 & 0 & 0 & 0 & 0 & 0 & 0 & 1 & 1 & 0 & 0 & 1 & 1 & 0 \\ 0 & 0 & 0 & 0 & 0 & 0 & 0 & 0 & 0 & 0 & 0 & 1 & 1 & 0 & 0 & 1 & 1 \\ 0 & 0 & 0 & 0 & 0 & 0 & 0 & 0 & 1 & 0 & 0 & 0 & 1 & 0 & 0 & 0 & 1 \\ 0 & 0 & 1 & 1 & 0 & 1 & 1 & 0 & 0 & 1 & 1 & 0 & 0 & 1 & 1 & 0 & 0 \end{bmatrix} \quad (A4)$$

As described in [48], encoding of CSS codewords may be performed with a row-reduced parity-check matrix without permuting the columns (ordering of data qubits) as may be required to put the parity-check matrix in systematic form. A row-reduced parity-check matrix for H_Q is given by

$$H_Q^r = \begin{bmatrix} 1 & 0 & 0 & 1 & 0 & 1 & 0 & 0 & 0 & 1 & 0 & 0 & 1 & 0 & 1 & 1 & 1 \\ 0 & 1 & 0 & 1 & 0 & 0 & 0 & 0 & 0 & 0 & 0 & 0 & 1 & 1 & 0 & 0 & 0 \\ 0 & 0 & 1 & 1 & 0 & 1 & 0 & 0 & 0 & 1 & 0 & 0 & 0 & 1 & 1 & 1 & 1 \\ 0 & 0 & 0 & 0 & 1 & 1 & 0 & 0 & 0 & 0 & 0 & 0 & 0 & 1 & 1 & 0 & 0 \\ 0 & 0 & 0 & 0 & 0 & 0 & 1 & 0 & 0 & 0 & 0 & 0 & 1 & 0 & 0 & 1 & 0 \\ 0 & 0 & 0 & 0 & 0 & 0 & 0 & 1 & 0 & 0 & 0 & 0 & 1 & 0 & 0 & 0 & 1 \\ 0 & 0 & 0 & 0 & 0 & 0 & 0 & 0 & 1 & 0 & 0 & 0 & 1 & 0 & 0 & 0 & 1 \\ 0 & 0 & 0 & 0 & 0 & 0 & 0 & 0 & 0 & 1 & 1 & 0 & 0 & 1 & 1 & 0 & 0 \end{bmatrix} \quad (A5)$$

Generators for the stabilizer and the normalizer of the $[[17, 1, 5]]$ color code are shown in Table V and Table VI, respectively. Since the minimum weight of the non-stabilizer elements of the normalizer is the distance of the code, from Table VI, we see that $d_Q = 5$. If a stabilizer has weight less than the code distance, the code is degenerate. From Table V, we conclude that the $[[17, 1, 5]]$ is degenerate since, for example, $wt(X_1X_2X_3X_4) = 4 < d_Q$.

Degenerate codes have multiple error patterns mapping to the same syndrome measurement which all lie in the same coset under the stabilizer group action. A many-to-one mapping of error patterns to syndromes may introduce ambiguity in designing a decoder, nonetheless a lookup table for the $[[17, 1, 5]]$ may be tabulated by evaluating the syndromes for all low-weight (≤ 2) error patterns. There are $17 + \binom{17}{2} = 136$ error patterns of weight less than or equal to $t_Q = 2$. An enumeration of bit-flip cosets is shown in Table VII. Note that due to degeneracy, there are only 115 distinct syndromes corresponding to all weight-1 and 2 error patterns.

s_X	s_Z	r_X	r_Z
$X_1X_2X_3X_4$	$Z_1Z_2Z_3Z_4$	$X_1X_4X_6X_{10}X_{13}X_{15}X_{16}X_{17}$	$Z_1Z_4Z_6Z_{10}Z_{13}Z_{15}Z_{16}Z_{17}$
$X_1X_3X_5X_6$	$Z_1Z_3Z_5Z_6$	$X_2X_4X_{13}X_{14}$	$Z_2Z_4Z_{13}Z_{14}$
$X_5X_6X_9X_{10}$	$Z_5Z_6Z_9Z_{10}$	$X_3X_4X_6X_{10}X_{14}X_{15}X_{16}X_{17}$	$Z_3Z_4Z_6Z_{10}Z_{14}Z_{15}Z_{16}Z_{17}$
$X_7X_8X_{11}X_{12}$	$Z_7Z_8Z_{11}Z_{12}$	$X_5X_6X_{13}X_{14}$	$Z_5Z_6Z_{13}Z_{14}$
$X_9X_{10}X_{13}X_{14}$	$Z_9Z_{10}Z_{13}Z_{14}$	$X_7X_{12}X_{15}X_{17}$	$Z_7Z_{12}Z_{15}Z_{17}$
$X_{11}X_{12}X_{15}X_{16}$	$Z_{11}Z_{12}Z_{15}Z_{16}$	$X_8X_{12}X_{16}X_{17}$	$Z_8Z_{12}Z_{16}Z_{17}$
$X_8X_{12}X_{16}X_{17}$	$Z_8Z_{12}Z_{16}Z_{17}$	$X_9X_{10}X_{13}X_{14}$	$Z_9Z_{10}Z_{13}Z_{14}$
$X_3X_4X_6X_7X_{10}X_{11}X_{14}X_{15}$	$Z_3Z_4Z_6Z_7Z_{10}Z_{11}Z_{14}Z_{15}$	$X_{11}X_{12}X_{15}X_{16}$	$Z_{11}Z_{12}Z_{15}Z_{16}$

TABLE V. Generators of the stabilizer of the $[[17, 1, 5]]$ color code in the planar basis g (see Fig. 9 and (A4)) and the row-reduced basis h (A5)

η_X	η_Z
$X_1X_2X_3X_4$	$Z_1Z_2Z_3Z_4$
$X_1X_3X_5X_6$	$Z_1Z_3Z_5Z_6$
$X_1X_3X_9X_{10}$	$Z_1Z_3Z_9Z_{10}$
$X_7X_8X_{11}X_{12}$	$Z_7Z_8Z_{11}Z_{12}$
$X_1X_2X_5X_9X_{13}$	$Z_1Z_2Z_5Z_9Z_{13}$
$X_2X_3X_5X_9X_{14}$	$Z_2Z_3Z_5Z_9Z_{14}$
$X_1X_3X_7X_{11}X_{15}$	$Z_1Z_3Z_7Z_{11}Z_{15}$
$X_1X_3X_8X_{11}X_{16}$	$Z_1Z_3Z_8Z_{11}Z_{16}$
$X_1X_3X_7X_8X_{17}$	$Z_1Z_3Z_7Z_8Z_{17}$

TABLE VI. Generators of the normalizer of the $[[17, 1, 5]]$ color code. All weight-4 generators are elements of the stabilizer.

The coset table also serves as a lookup table decoder for the $[[17, 1, 5]]$ since any element of coset can correct any other element in the coset. Take, for example, the coset of errors

$$E = \{X_1X_3, X_2X_4, X_5X_6, X_9X_{10}, X_{13}X_{14}\} \quad (\text{A6})$$

which all trigger the syndrome measurement “10100000”. The product of any two elements of E lies in the stabilizer and can therefore be corrected by a single Pauli- X operator. For example, the product

$$X_1X_3X_9X_{10} \quad (\text{A7})$$

can be written as a product of generators $r_1r_3r_7$:

$$r_1r_3 = X_1X_3X_{13}X_{14} \quad (\text{A8})$$

$$r_1r_3r_7 = X_1X_3X_{13}X_{14}X_9X_{10}X_{13}X_{14} \quad (\text{A9})$$

$$= X_1X_3X_9X_{10} \quad (\text{A10})$$

The correction X_1X_3 therefore corrects an error X_1X_3 but also the error X_9X_{10} . Similar decomposition of products from E may be computed and it can be shown that any element of E may be chosen as the corrective action to any other element of E .

10000000	X_1	01000000	X_2	00100000	X_3
11100000	X_4	00010000	X_5	10110000	X_6
00001000	X_7	00000100	X_8	00000010	X_9
10100010	X_{10}	00000001	X_{11}	00001101	X_{12}
11010010	X_{13}	01110010	X_{14}	10101001	X_{15}
10100101	X_{16}	10101100	X_{17}		
11000000	X_1X_2, X_3X_4	10100000	$X_1X_3, X_2X_4, X_5X_6, X_9X_{10}, X_{13}X_{14}$	01100000	X_1X_4, X_2X_3
00110000	X_1X_6, X_3X_5	10001000	X_1X_7	10000100	X_1X_8
10000010	X_1X_9, X_3X_{10}	00100010	X_1X_{10}, X_3X_9	10000001	X_1X_{11}
10001101	X_1X_{12}	01010010	X_1X_{13}, X_3X_{14}	11110010	X_1X_{14}, X_3X_{13}
00101001	X_1X_{15}	00100101	X_1X_{16}	00101100	X_1X_{17}
01010000	X_2X_5, X_4X_6	11110000	X_2X_6, X_4X_5	01001000	X_2X_7
01000100	X_2X_8	01000010	X_2X_9, X_4X_{10}	11100010	X_2X_{10}, X_4X_9
01000001	X_2X_{11}	01001101	X_2X_{12}	10010010	X_2X_{13}, X_4X_{14}
00110010	X_2X_{14}, X_4X_{13}	11101001	X_2X_{15}	11100101	X_2X_{16}
11101100	X_2X_{17}	00101000	X_3X_7	00100100	X_3X_8
00100001	X_3X_{11}	00101101	X_3X_{12}	10001001	X_3X_{15}
10000101	X_3X_{16}	10001100	X_3X_{17}	11101000	X_4X_7
11100100	X_4X_8	11100001	X_4X_{11}	11101101	X_4X_{12}
01001001	X_4X_{15}	01000101	X_4X_{16}	01001100	X_4X_{17}
00011000	X_5X_7	00010100	X_5X_8	00010010	X_5X_9, X_6X_{10}
10110010	X_5X_{10}, X_6X_9	00010001	X_5X_{11}	00011101	X_5X_{12}
11000010	X_5X_{13}, X_6X_{14}	01100010	X_5X_{14}, X_6X_{13}	10111001	X_5X_{15}
10110101	X_5X_{16}	10111100	X_5X_{17}	10111000	X_6X_7
10110100	X_6X_8	10110001	X_6X_{11}	10111101	X_6X_{12}
00011001	X_6X_{15}	00010101	X_6X_{16}	00011100	X_6X_{17}
00001100	$X_7X_8, X_{11}X_{12}, X_{15}X_{16}$	00000100	X_7X_9	10101010	X_7X_{10}
00001001	$X_7X_{11}, X_8X_{12}, X_{16}X_{17}$	00000101	$X_7X_{12}, X_8X_{11}, X_{15}X_{17}$	11011010	X_7X_{13}
01111010	X_7X_{14}	10100001	$X_7X_{15}, X_8X_{16}, X_{12}X_{17}$	10101101	$X_7X_{16}, X_8X_{15}, X_{11}X_{17}$
10100100	$X_7X_{17}, X_{11}X_{16}, X_{12}X_{15}$	000000110	X_8X_9	10100110	X_8X_{10}
11010110	X_8X_{13}	01110110	X_8X_{14}	10101000	$X_8X_{17}, X_{11}X_{15}, X_{12}X_{16}$
00000011	X_9X_{11}	00000111	X_9X_{12}	11010000	$X_9X_{13}, X_{10}X_{14}$
01110000	$X_9X_{14}, X_{10}X_{13}$	10101011	X_9X_{15}	10100111	X_9X_{16}
10101110	X_9X_{17}	10100011	$X_{10}X_{11}$	10101111	$X_{10}X_{12}$
00001011	$X_{10}X_{15}$	000000111	$X_{10}X_{16}$	000001110	$X_{10}X_{17}$
11010011	$X_{11}X_{13}$	01110011	$X_{11}X_{14}$	11011111	$X_{12}X_{13}$
01111111	$X_{12}X_{14}$	01111011	$X_{13}X_{15}$	01110111	$X_{13}X_{16}$
01111110	$X_{13}X_{17}$	11011011	$X_{14}X_{15}$	11010111	$X_{14}X_{16}$
11011110	$X_{14}X_{17}$	10010000	X_1X_5, X_3X_6		

TABLE VII. Lookup table for weight-1 and 2 bit-flips for the $[[17, 1, 5]]$ color code.

Appendix B: Bit-flip example cosets and lookup table

000	X_3	X_6	X_9	X_{12}	X_1X_2	X_4X_5	X_7X_8	$X_1X_7X_{10}$	$X_1X_7X_{11}$
101	X_1	X_1X_3	X_1X_6	X_1X_9	X_1X_{12}	X_2	$X_1X_4X_5$	$X_1X_7X_8$	X_7X_{10}
110	X_7	X_3X_7	X_6X_7	X_7X_9	X_7X_{12}	$X_1X_2X_7$	$X_4X_5X_7$	X_8	X_1X_{10}
011	X_{10}	X_{11}	X_6X_{10}	X_9X_{10}	$X_{10}X_{12}$	$X_1X_2X_{10}$	$X_4X_5X_{10}$	$X_7X_8X_{10}$	X_1X_7
111	X_4	X_3X_4	X_4X_6	X_4X_9	X_4X_{12}	$X_1X_2X_4$	X_5	$X_4X_7X_8$	$X_1X_4X_7X_{10}$

TABLE VIII. Cosets of \mathcal{P}_{12} under the action of $\mathbf{A}^\top \otimes [110]$

000	X_2	X_5	X_8	X_{11}	X_1X_3	X_4X_6	X_7X_9	$X_1X_7X_{10}$	$X_1X_7X_{12}$
101	X_1	X_1X_2	X_1X_5	X_1X_8	X_1X_{11}	X_3	$X_1X_4X_6$	$X_1X_7X_9$	X_7X_{10}
110	X_7	X_2X_7	X_5X_7	X_7X_8	X_7X_{11}	$X_1X_3X_7$	$X_4X_6X_7$	X_9	X_1X_{10}
011	X_{10}	X_2X_{10}	X_5X_{10}	X_8X_{10}	$X_{10}X_{11}$	$X_1X_3X_{10}$	$X_4X_6X_{10}$	$X_7X_9X_{10}$	X_1X_7
111	X_4	X_2X_4	X_4X_5	X_4X_8	X_4X_{11}	$X_1X_3X_4$	X_6	$X_4X_7X_9$	$X_1X_4X_7X_{10}$

TABLE IX. Cosets of \mathcal{P}_{12} under the action of $\mathbf{A}^\top \otimes [101]$

101000	$\textcolor{red}{X_2}$	X_8X_{11}	$X_1X_9X_{12}$	$X_3X_7X_{10}$
000101	X_3	X_9X_{12}	$X_1X_8X_{11}$	$X_2X_7X_{10}$
110000	X_8	X_2X_{11}	$X_1X_9X_{10}$	$X_3X_7X_{12}$
000110	X_9	X_3X_{12}	$X_1X_8X_{10}$	$X_2X_7X_{11}$
011000	X_{11}	X_2X_8	$X_1X_7X_{12}$	$X_3X_9X_{10}$
000011	X_{12}	X_3X_9	$X_1X_7X_{11}$	$X_2X_8X_{10}$
111000	X_5	$X_1X_5X_7X_{10}$	$X_2X_5X_8X_{11}$	$X_3X_5X_9X_{12}$
000111	X_6	$X_1X_6X_7X_{10}$	$X_2X_6X_8X_{11}$	$X_3X_6X_9X_{12}$
101101	X_1	X_7X_{10}	$X_2X_9X_{12}$	$X_3X_8X_{11}$
110110	$\textcolor{blue}{X_7}$	$\textcolor{green}{X_1X_{10}}$	$X_2X_9X_{11}$	$X_3X_8X_{12}$
011011	X_{10}	X_1X_7	$X_2X_8X_{12}$	$X_3X_9X_{11}$
111111	X_4	$X_1X_4X_7X_{10}$	$X_2X_4X_8X_{11}$	$X_3X_4X_9X_{12}$

TABLE X. Look-up table decoder for the three-qubit bit-flip code encoded with the parity-check matrix \mathbf{A}^\top of the classical $[7, 4, 3]$ Hamming code formed by joining Tables VIII and IX. A unique syndrome exists for any single bit-flip occurring in the data qubits. Highlighted are the syndromes corresponding to bit-flips X_2 (red) and X_7 (blue) and the weight-2 error X_1X_{10} (green) as depicted in the stabilizer circuits in Figs. 1 and 2.